Joint Beamforming Aided Over-the-Air Computation Systems Relying on Both BS-Side and User-Side Reconfigurable Intelligent Surfaces

Xiongfei Zhai, *Member, IEEE,* Guojun Han, *Senior Member, IEEE,*
Yunlong Cai, *Senior Member, IEEE,* and Lajos Hanzo, *Fellow, IEEE*

***Abstract*—Over-the-air computation (AirComp) has received substantial attention, given its ability to aggregate massive amounts of data from distributed wireless devices (WDs). However, the computation accuracy at the fusion center (FC) may be severely affected by receiving data corrupted by the poor channel conditions. To mitigate this issue, we consider the employment of reconfigurable intelligent surfaces (RISs) in the AirComp system considered for improving the quality of received data, and hence improve the computation accuracy. However, most previous contributions on RIS-assisted AirComp systems only employ a single RIS in the resultant single-RIS-assisted (SRIS-assisted) AirComp systems. We develop this concept further for mitigating the deleterious channel effects by conceiving a double-RIS-assisted (DRIS-assisted) AirComp system, where one of the RISs is located near the WDs and the other in the vicinity of the FC. We theoretically prove that the DRIS-assisted AirComp system outperforms its SRIS-assisted counterpart in terms of the resultant computation mean-squared-error (MSE). Furthermore, we propose a pair of algorithms for jointly optimizing the transmit power at the WDs, the receive beamforming vector at the FC, and the passive beamforming matrices at the RISs for minimizing the computational MSE. Specifically, the transmit power is updated by exploiting the Lagrange duality method, while the receive beamforming vector is optimized by utilizing the first-order optimality condition. Furthermore, a pair of techniques are developed for optimizing the passive beamforming matrices at the RISs based on semidefinite relaxation (SDR) and penalty-duality-decomposition (PDD), respectively. Both the complexity and the convergence of the proposed algorithms are analyzed. Finally, simulation results are provided for quantifying the overall performance of the resultant DRIS-assisted AirComp system.**

***Index Terms*—Over-the-air computation (AirComp), Internet-of-Things (IoT) networks, double reconfigurable intelligent surfaces (DRIS).**

The work of X. Zhai was supported in part by the Technology Program of Guangzhou under Grant 202102020869, and the Guangdong Basic and Applied Basic Research Foundation under Grants 2022A1515010153 and 2021A1515011645. The work of G. Han was supported in part by the Joint Funds of the National Natural Science Foundation of China and Guangdong under Grant U2001203, and the National Natural Science Foundation of China under Grant 61871136. The work of Y. Cai was supported in part by the National Natural Science Foundation of China under Grants 61971376 and 61831004, and in part by the Zhejiang Provincial Natural Science Foundation for Distinguished Young Scholars under Grant LR19F010002. L. Hanzo would like to acknowledge the financial support of the Engineering and Physical Sciences Research Council projects EP/P034284/1 and EP/P003990/1 (COALESCE) as well as of the European Research Council's Advanced Fellow Grant QuantCom (Grant No. 789028). (Corresponding author: Yunlong Cai)

X. Zhai and G. Han are with the School of Information Engineering, Guangdong University of Technology, Guangzhou 510006, China (e-mail: zhaixiongfei@gdut.edu.cn; gjhan@gdut.edu.cn).

Y. Cai is with the College of Information Science and Electronic Engineering, Zhejiang University, Hangzhou 310027, China (e-mail: ylcai@zju.edu.cn).

L. Hanzo is with the Department of Electronics and Computer Science, University of Southampton, Southampton, UK (Email: lh@ecs.soton.ac.uk).

I. Introduction

In the Internet-of-things (IoT) networks, the ultra-fast aggregation of massive amounts of data from a large number of wireless devices (WDs) is becoming an urgent demand [1], [2], [11]. However, conventional communication systems tend to falter in the face of this challenge due to the fact that the fusion center (FC) has to restore the individual data stream of each WD before aggregating them. Some of the impediments in conventional communication systems are: 1) the data recovery of each WD suffers from inter-WD interference; 2) its latency may be excessive; 3) as the number of WDs increases, the spectral- and energy-efficiency of conventional systems erodes. Bearing in mind that the FC generally focuses on computing a specific function (e.g. the weighted sum, the arithmetic mean, or the geometric mean) in practical IoT network applications, over-the-air computation (AirComp) has been recognized as a promising solution [4]–[13]. In contrast to the traditional communication systems which treat the inter-WD interference as a harmful factor, AirComp beneficially exploits the co-channel interference arriving from different WDs to assist the computations. Based on the signal superposition introduced by the wireless channels, AirComp enables the FC to directly compute the aforementioned nomographic functions. Therefore, AirComp can be exploited in diverse applications, such as distributed sensing, distributed consensus control and federated learning [14]. In the areas of distributed sensing and federated learning, typically the computation of arithmetic mean is required. For instance, the unmanned aerial vehicles (UAVs) equipped with AirComp may obtain the average temperature, humidity, and noise by collecting the data from distributed sensors mounted on buildings for ubiquitous city surveillance in smart-city applications. Alternatively, a server in federated learning can update its global model with the average of the models from all the edge devices by exploiting AirComp. Furthermore, UAV swarm formation control and vehicular platooning relying on distributed consensus control can be achieved upon supporting all vehicles by AirComp and then updating the individual information state of each vehicle with the average of those of others.

In AirComp systems typically the computation mean-squared error (MSE) is used as the main accuracy metric. Since it was shown in [15] that the optimal computation accuracy may be achieved for independently and identically Gaussian distributed data sources by simple analog wireless transmission in AirComp systems, the computation MSE was quantified in [4]–[13]. For the scenario where the FC and WDs are all equipped with a single antenna and fading channels are

assumed, the authors of [4]–[6] studied the optimal power allocation algorithm of AirComp systems based on popular convex optimization techniques. As a further advance, with the objective of minimizing the outage probability (defined as the probability that the computation MSE exceeds a given threshold), the authors of [7] investigated the corresponding optimal power control strategy. To facilitate multi-functional computation in AirComp, multi-input multi-output (MIMO) techniques have also been exploited. In particular, a MIMO-aided AirComp system was studied in [9], where a zero-forcing (ZF) based beamformer was proposed for minimizing the multi-functional computation MSE. In [10], the technique of orthogonal frequency division multiplexing (OFDM) was considered in AirComp and a sub-function allocation of sub-carriers was proposed to prevent a vanishing computation rate from the increase in the number of WDs. Since accurate time synchronization is important for AirComp to achieve low computation MSE, the authors of [12] developed a synchronization scheme, namely AirShare, where a shared block is broadcast by the FC to all WDs for synchronization.

However, as the number of the WDs increases, the computation accuracy of AirComp is significantly affected by the WDs having poor channel conditions. For mitigating this potential performance erosion, massive MIMO techniques were proposed for AirComp in [13], [16], [17]. In particular, the authors of [16] formulated a hybrid analog-digital (AD) beamforming design problem for their massive MIMO AirComp system and developed a successive-convex-approximation (SCA) based algorithm. Furthermore, it was proven that the computation MSE is inversely proportional to the number of receive antennas. For a large number of WDs an AirComp system relying on non-orthogonal multiple access (NOMA) was conceived in [18], where the different functions of WDs were allocated to different resource blocks. Although the above techniques improve the computational performance of AirComp, this is typically achieved at an excessive energy consumption and complexity. Hence, efficiently reducing the computation MSE of AirComp remains an open problem.

Recently, sophisticated reconfigurable intelligent surfaces (RIS) have been proposed for increasing the spatial degrees of freedom (DoF), hence attaining significant array gains at a low energy consumption and complexity [19]–[23]. They rely on passive reflecting elements adjusting the phase shift and even potentially the amplitude of the incident signal for creating a favorable propagation environment. This is achieved without requiring any radio frequency (RF) chains, which leads to reduced fabrication cost and energy consumption as compared to that of massive MIMO techniques. As a further benefit, the authors of [24] demonstrated that there is no need for upgrading the existing infrastructure when incorporating RISs in the existing systems. Given the above advantages, RISs have received special attention in various areas, including RIS-assisted physical layer security [25]–[27], RIS-aided wireless power transfer [28]–[32], and RIS-assisted OFDM [33], [34], etc. Furthermore, RIS-assisted AirComp systems have also been studied in [35]–[38]. Specifically, to tackle the joint active and passive beamforming problem of RIS-assisted AirComp systems, the authors of [35] proposed a novel beamforming algorithm based on difference-of-convex (DC) programming and matrix lifting. Moreover, a RIS-assisted AirComp system relying on energy-harvesting was investigated in [37], which consists of an energy beamforming phase and an AirComp phase, leading to a pair of subproblems. These subproblems were solved separately by exploiting semidefinite relaxation (SDR) and DC programming, respectively. These contributions have also demonstrated that the computation accuracy of AirComp is significantly enhanced by RISs.

Nevertheless, the above treatises do not consider the hostile RIS-assisted AirComp scenario, where the direct link between the WDs and the FC is unavailable. In this scenario relying on single-RIS deployment may not succeed in sufficiently improving the AirComp performance. As a remedy, a pair of RISs has been proposed in [39]–[41] for conceiving a superior architecture. Explicitly, one of the RISs is placed near the base station (BS) and the other near the users for the sake of providing multiplicative beamforming gain, when the direct link is blocked by obstacles. The benefits of this pair of BS-side and user-side RISs might be viewed as being reminiscent of echoing those of ingeniously harnessing a pair of convolutional codes for creating a powerful turbo code or using a pair of specifically combined antennas to create a space-time code. In this spirit, a joint active and passive beamforming design was proposed based on alternating optimization and maximum-ratio combining (MRC), where SDR was proposed for maximizing the minimum signal-to-interference-plus-noise ratio (SINR) at the receiver of both single- and multi-user MIMO systems. Accurate channel estimation is indispensable in this double-RIS-assisted (DRIS-assisted) MIMO system for increasing the passive beamforming gain, but this is more challenging than that of single-RIS-assisted (SRIS-assisted) MIMO systems.

To tackle this issue, the authors of [40], [41] developed an efficient channel estimation scheme for DRIS-assisted MIMO systems, which treat the cascaded channel coefficients between the BS and the users as the scaled versions of their super-imposed lower-dimensional channel state information (CSI). All the above treatises proved that the employment of two RISs can achieve higher passive beamforming gains than a single RIS. However, double-RIS assisted AirComp has not been reported in the open literature. **In contrast to [39]–[41], the DRIS-assisted AirComp proposed harnesses the interference as a beneficial factor, which leads to completely new joint active and passive beamforming optimization problems and solutions.**

Explicitly, the contributions of this paper are summarized as follows.

- We investigate a DRIS-assisted AirComp system relying on a multi-antenna FC, a pair of RISs, and a high number of single-antenna WDs, which computes the sum of the data gleaned from the WDs. The direct link between the FC and the WDs is assumed to be unavailable and the WDs have to transmit the data to the FC via the single-reflection and double-reflection links. Thus the transmit coefficients at the WDs, the passive beamforming matrices at the RISs, and the receive beamforming vector at

the FC have to be jointly optimized for minimizing the computation MSE. This challenging problem is generally intractable.

- We seek to solve this problem in an alternating manner. In particular, the transmit power at the WDs and the receive beamforming vector at the FC are optimized by exploiting the Lagrange duality method and the first-order optimality condition, respectively. Inspired by [39] and [42], the passive beamforming matrices are updated based on the SDR and penalty-duality-decomposition (PDD) methods. We also analyze the convergence and computational complexity of the proposed algorithms.
- To gain more insights, by assuming that the number of passive reflecting elements and that of the receive antennas are both sufficiently large, we prove that the computation MSE of the DRIS-assisted AirComp system is lower than that of the SRIS-assisted one.
- Compared to other benchmarks relying on the block coordinate descent (BCD) and Manifold optimization methods, our numerical results show that the proposed algorithms substantially reduce the computation MSE of the DRIS-assisted AirComp system.

The rest of this paper is organized as follows. Section II presents the system model and problem formulation for the DRIS-assisted AirComp system. In Section III, we propose the DRIS-SDR and DRIS-PDD algorithms to solve the formulated problem and analyze their convergence and complexity. Section IV proves that the computation MSE of the DRIS-assisted AirComp system is less than that of the SRIS-assisted one. Section V shows the numerical results. Finally, Section VI offers our conclusions.

Notations: Throughout this paper, we adopt bold upper-case letters for matrices and bold lower-case letters for vectors. The other notations in this paper are summarized in Table I.

TABLE I: The notations appeared in the paper.

Notation	Meaning
$\mathbf{A}(i,j)$	The entry on the i^{th} row and the j^{th} column of $\mathbf{A}$
$\mathbf{A}^*$	The conjugate of $\mathbf{A}$
$\mathbf{A}^T$	The transpose of $\mathbf{A}$
$\mathbf{A}^H$	The Hermitian transpose of $\mathbf{A}$
$\mathbf{I}$	The identity matrix
$\mathbb{C}^{m\times n}$	The m-by-n dimensional complex space
$\mathbb{E}(\cdot)$	The expectation
$\mathrm{Tr}(\cdot)$	The trace
$\|\cdot\|$	The Frobenius norm
$\|\cdot\|_\infty$	The infinite norm
$\mathcal{CN}(\boldsymbol{\Upsilon},\boldsymbol{\Phi})$	The circularly symmetric complex Gaussian (CSCG) distribution with mean $\boldsymbol{\Upsilon}$ and covariance matrix $\boldsymbol{\Phi}$
$\mathrm{mod}(a,b)$	The modulus operation of a with respect to b

II. System Description

In this section, we first introduce the system model and channel model for the DRIS-assisted AirComp system. Then the optimization problem of interest is mathematically formulated.

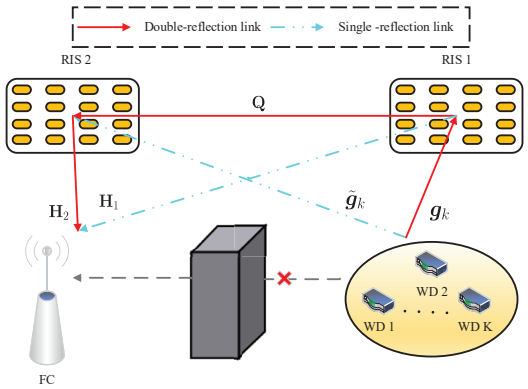

Fig. 1: DRIS-assisted AirComp system.

A. System Model

We investigate the DRIS-assisted AirComp system of Fig. 1, where both a BS-side and a user-side RISs are employed for supporting both the communications and computations of K single-antenna WDs and an N-antenna FC. In particular, the FC is equipped with a uniform linear array (ULA). Each WD first collects its own heterogeneous time-varying parameters (e.g., humidity, temperature, noise) of the environment, and then all WDs simultaneously transmit the collected data to the FC for functional computation. In this paper, we consider a practical scenario where the WDs cannot transmit signals to the FC via the direct links due to obstacles (e.g., walls, corners, and buildings) and thus the direct links are ignored [1]. To bypass the obstacles and reduce the path loss, a pair of RISs, i.e., RIS 1 and RIS 2, are appropriately located near the WDs and the FC, respectively. Thus, the FC receives the transmitted signals from the WDs through both the single- and double-reflection links with the aid of two RISs [2]. We assume that RIS 1 and RIS 2 consist of M_1 and M_2 passive reflecting elements, respectively, and the total number of passive reflecting elements is denoted by $M = M_1 + M_2$. Furthermore, the RISs employ the uniform planar array (UPA) with $M_1 = M_{y,1}M_{z,1}$ and $M_2 = M_{y,2}M_{z,2}$, where $M_{y,1}$ ($M_{y,2}$) and $M_{z,1}$ ($M_{z,2}$) denote the number of passive reflecting elements on the y- and z-axis, respectively. For convenience, we denote $\mathcal{K} \triangleq \{1,2,\ldots,K\}$, $\mathcal{N} \triangleq \{1,2,\ldots,N\}$, and $\mathcal{M}_\mu \triangleq \{1,2,\ldots,M_\mu\}$, where $\mu \in \{1,2\}$, as the sets of WDs, receive antennas at the FC and passive reflecting elements at the RIS, respectively. We assume that the synchronization of different WDs relies on accurate timing advance control mechanism based on propagation delay estimation and transmission ahead of time, which is commonly used in long term evolution (LTE) systems [14].

At a particular time slot (TS), the data collected by WD $k \in \mathcal{K}$ is denoted by $s_k \in \mathbb{C}$, which are independent of each other,

[1]The FC and the WDs can obtain this information by performing the conventional channel estimation method based on uplink/downlink training and channel reciprocity with the two RISs both turned off [43], [44]. From the obtained CSI of the direct links, if the pathloss is extremely large, the FC and the WDs know that the direct links are blocked and can be negligible.

[2]The higher order reflection is neglected due to the large energy attenuation.

i.e. we have $\mathbb{E}(s_k s_k^*) = 1,\ \mathbb{E}(s_k s_j^*) = 0,\ \forall k,\ j \in \mathcal{K},\ k \neq j$ [3]. Based on the superposition of the wireless multiple access channel, the FC is capable of directly computing the sum function (i.e., $s = \sum_{k\in\mathcal{K}} s_k$) of the data gleaned from all WDs at a reduced communication overhead for prompt data aggregation [9]. We would like to note that this design can be readily extended to other nomographic functions [46]. According to the investigated system model, by denoting $v_k \in \mathbb{C}$ as the transmit coefficient at the WD k with the transmit power constraint $|v_k|^2 \leq P,\ \forall k \in \mathcal{K}$, the transmitted signal by the WD k is given by

$$x_k = v_k s_k. \tag{1}$$

Let $\boldsymbol{\theta}_\mu \triangleq [\theta_{\mu,1}, \ldots, \theta_{\mu,M_\mu}]^T = [\exp(j\phi_{\mu,1}), \ldots, \exp(j\phi_{\mu,M_\mu})]^T \in \mathbb{C}^{M_\mu \times 1}$ denote the equivalent passive beamforming vector of RIS μ with $\mu \in \{1, 2\}$, where $\phi_{\mu,m} \in [0, 2\pi]$ is the phase shift of passive reflecting element m at RIS μ, respectively. Therefore, the vector of received signal at the FC is given by

$$\boldsymbol{y} = \sum_{k\in\mathcal{K}} (\underbrace{\mathbf{H}_2\boldsymbol{\Theta}_2\mathbf{Q}\boldsymbol{\Theta}_1\boldsymbol{g}_k}_{\text{double-reflection link}} + \underbrace{\mathbf{H}_2\boldsymbol{\Theta}_2\tilde{\boldsymbol{g}}_k + \mathbf{H}_1\boldsymbol{\Theta}_1\boldsymbol{g}_k}_{\text{single-reflection links}}) v_k s_k + \boldsymbol{n}, \tag{2}$$

where $\boldsymbol{g}_k \in \mathbb{C}^{M_1\times 1}$, $\tilde{\boldsymbol{g}}_k \in \mathbb{C}^{M_2\times 1}$, $\mathbf{H}_1 \in \mathbb{C}^{N\times M_1}$, $\mathbf{H}_2 \in \mathbb{C}^{N\times M_2}$, and $\mathbf{Q} \in \mathbb{C}^{M_2\times M_1}$ denote the channel vectors/matrices from WD k to RIS 1, from WD k to RIS 2, from RIS 1 to the FC, from RIS 2 to the FC, and from RIS 1 to RIS 2, respectively. $\boldsymbol{\Theta}_\mu = \text{diag}(\boldsymbol{\theta}_\mu^*) \in \mathbb{C}^{M_\mu\times M_\mu}$ is the diagonal passive beamforming matrix of RIS μ with $\mu \in \{1, 2\}$. $\boldsymbol{n} \in \mathbb{C}^{N\times 1}$ represents the additive white Gaussian noise (AWGN) vector with $\boldsymbol{n} \sim \mathcal{CN}(\mathbf{0}, \sigma^2\mathbf{I})$. Note that the CSI of single- and double-reflection links are assumed to be known at the FC and the WDs. The CSI can be obtained by applying the channel estimation scheme in [40]. In particular, for an arbitrary WD, the superimposed CSI of the single- and double-reflection links related to RIS 2 is derived and estimated by dynamically tuning reflection phase-shifts of RIS 2 and fixing those of RIS 1. Due to the fact that the cascaded channel coefficients of the single- and double-reflection links are scaled versions of their superimposed CSI, they can be efficiently estimated. Similarly, the CSI of WD–RIS 1–FC links can be also estimated. For other WDs, their cascaded channels are also scaled versions of the given CSI of arbitrary WD. Hence, they can be estimated efficiently. The problem of analysing the impact of imperfect CSI for the DRIS-assisted AirComp system is also new and worth investigating, which will be left for our future work.

By letting $\boldsymbol{u} \in \mathbb{C}^{N\times 1}$ denote the receive beamforming vector at the FC, the restored signal after the receive beamforming is given by $\hat{s} = \boldsymbol{u}^H\boldsymbol{y}$.

[3]The independent data sources are considered in this work for the ease of analysis, as commonly considered in the literature, e.g., [9] and [13]. With the given covariance between the collected data from different WDs, our proposed algorithm can be extended into the case in which the data sources are correlated.

B. Channel Model

We consider a general spatially correlated Rician fading channel model for $\boldsymbol{g}_k$, $\tilde{\boldsymbol{g}}_k$, $\mathbf{H}_1$, $\mathbf{H}_2$, and $\mathbf{Q}$ in this paper with $k \in \mathcal{K}$. There are two main components in this channel model, namely the line-of-sight (LoS) and non-LoS (NLoS) components, where the LoS components depend on the locations of the WDs, the RISs, and the FC. Moreover, we assume that the second-order statistics of the LoS components are identical for each WD. In the following, we formulate the channel vector from WD k to RIS 1 according to the investigated model as

$$\boldsymbol{g}_k = \sqrt{\frac{\beta_{WR_1}}{1+\beta_{WR_1}}}\bar{\boldsymbol{z}}_{g,k} + \sqrt{\frac{1}{1+\beta_{WR_1}}}\boldsymbol{z}_{g,k}, \tag{3}$$

with $\bar{\boldsymbol{z}}_{g,k} \in \mathbb{C}^{M_1\times 1}$ and $\beta_{WR_1} \in \mathbb{R}$ being the LoS component and the Rician factor, respectively. $\boldsymbol{z}_{g,k} \in \mathbb{C}^{M_1\times 1}$ represents the NLoS component in $\boldsymbol{g}_k$ and follows the independently and identically Rayleigh fading distribution with $\boldsymbol{g}_k(m) \sim \mathcal{CN}(0, l_{k,1})$, where $l_{k,1,m}$ denotes the location-dependent path loss from WD k to the mth reflecting element of RIS 1. Similarly, the channel vectors/matrices from WD k to RIS 2, from RIS 1 to the FC, from RIS 2 to the FC, and from RIS 1 to RIS 2 are respectively given by

$$\tilde{\boldsymbol{g}}_k = \sqrt{\frac{\beta_{WR_2}}{1+\beta_{WR_2}}}\bar{\boldsymbol{z}}_{\tilde{g},k} + \sqrt{\frac{1}{1+\beta_{WR_2}}}\boldsymbol{z}_{\tilde{g},k}, \tag{4}$$

$$\mathbf{H}_1 = \sqrt{\frac{\beta_{R_1F}}{1+\beta_{R_1F}}}\bar{\mathbf{F}}_1 + \sqrt{\frac{1}{1+\beta_{R_1F}}}\mathbf{F}_1, \tag{5}$$

$$\mathbf{H}_2 = \sqrt{\frac{\beta_{R_2F}}{1+\beta_{R_2F}}}\bar{\mathbf{F}}_2 + \sqrt{\frac{1}{1+\beta_{R_2F}}}\mathbf{F}_2, \tag{6}$$

$$\mathbf{Q} = \sqrt{\frac{\beta_{RR}}{1+\beta_{RR}}}\bar{\mathbf{F}}_R + \sqrt{\frac{1}{1+\beta_{RR}}}\mathbf{F}_R, \tag{7}$$

where $\beta_{WR_2} \in \mathbb{R}$, $\beta_{R_1F} \in \mathbb{R}$, $\beta_{R_1F} \in \mathbb{R}$, and $\beta_{RR} \in \mathbb{R}$ denote the Rician factors for the WD–RIS 2, RIS 1–FC, RIS 2–FC, and RIS 1–RIS 2 links, respectively. $\bar{\boldsymbol{z}}_{\tilde{g},k} \in \mathbb{C}^{M_2\times 1}$, $\bar{\mathbf{F}}_1 \in \mathbb{C}^{N\times M_1}$, $\bar{\mathbf{F}}_2 \in \mathbb{C}^{N\times M_2}$, and $\bar{\mathbf{F}}_R \in \mathbb{C}^{M_2\times M_1}$ denote the LoS components, while $\boldsymbol{z}_{\tilde{g},k} \in \mathbb{C}^{M_2\times 1}$, $\mathbf{F}_1 \in \mathbb{C}^{N\times M_1}$, $\mathbf{F}_2 \in \mathbb{C}^{N\times M_2}$, and $\mathbf{F}_R \in \mathbb{C}^{M_2\times M_1}$ describe the channel Rayleigh fading, whose elements follow the distribution of $\mathcal{CN}(0, l_{k,2,m})$, $\mathcal{CN}(0, l_{1,m,n})$, $\mathcal{CN}(0, l_{2,m,n})$, and $\mathcal{CN}(0, l_{m,m})$, respectively, with $l_{k,2,m}$, $l_{1,m,n}$, $l_{2,m,n}$, and $l_{m,n}$ being the corresponding path loss. In particular, we respectively model the LoS components of the considered channel vectors/matrices, i.e., $\bar{\boldsymbol{z}}_{g,k}$, $\bar{\boldsymbol{z}}_{\tilde{g},k}$, $\bar{\mathbf{F}}_1$, $\bar{\mathbf{F}}_2$, and $\bar{\mathbf{F}}_R$, as follows

$$\begin{aligned}
&\bar{\boldsymbol{z}}_{g,k}(m) = \sqrt{l_{k,1,m}} f_1(\varphi_{k,1}, \psi_{k,1}), \forall m \in \mathcal{M}_1, k \in \mathcal{K},\\
&\bar{\boldsymbol{z}}_{\tilde{g},k}(m) = \sqrt{l_{k,2,m}} f_1(\varphi_{k,2}, \psi_{k,2}), \forall m \in \mathcal{M}_2, k \in \mathcal{K},\\
&\bar{\mathbf{F}}_1(m,n) = \sqrt{l_{1,m,n}} f_2(\vartheta_1) f_1(\varphi_1, \psi_1), \forall m \in \mathcal{M}_1, n \in \mathcal{N},\\
&\bar{\mathbf{F}}_2(m,n) = \sqrt{l_{2,m,n}} f_2(\vartheta_2) f_1(\varphi_2, \psi_2), \forall m \in \mathcal{M}_2, n \in \mathcal{N},\\
&\bar{\mathbf{F}}_R(m,n) = \sqrt{l_{m,n}} f_1(\varphi_a, \psi_a) f_1(\varphi_d, \psi_d),\\
&\forall m \in \mathcal{M}_2, n \in \mathcal{M}_1,
\end{aligned}$$

where $f_1(\varphi, \psi) \triangleq e^{j2\pi d_R \kappa_\mu/\lambda}$, $\kappa_\mu = (m - \lfloor m - M_{y,\mu}\rfloor M_{y,\mu})\sin(\varphi)\cos(\psi) + \lfloor m - M_{y,\mu}\rfloor \sin(\varphi)\sin(\psi)$ with

$\mu \in \{1,2\}$, and $f_2(\vartheta) \triangleq e^{j2\pi(n-1)d_F \sin(\vartheta)/\lambda}$. d_R and d_F denote the reflecting-element/antenna spacing at the RISs and the FC, respectively. λ represents the wavelength. $\varphi_{k,\mu}$ and $\psi_{k,\mu}$ denote the azimuth and elevation angles-of-arrival (AoAs) from WD k to RIS μ. ϑ_μ is the AoA from RIS μ to the FC. φ_μ and ψ_μ represent the azimuth and elevation angles-of-departure (AoDs) from RIS μ to the FC, respectively. φ_a (φ_d) and ψ_a (ψ_d) are the azimuth and elevation AoAs (AoDs) from RIS 1 to RIS 2.

C. Problem Formulation

The computation performance is usually measured by the MSE between $\hat{s}$ and s, which is given by

$$\begin{aligned}
&\zeta(\{v_k\}, \boldsymbol{\theta}_1, \boldsymbol{\theta}_2, \boldsymbol{u}) \\
&= \mathbb{E}(|\hat{s} - s|^2) \\
&= \sum_{k\in\mathcal{K}} |\boldsymbol{u}^H(\mathbf{H}_2\boldsymbol{\Theta}_2\mathbf{Q}\boldsymbol{\Theta}_1\boldsymbol{g}_k + \mathbf{H}_2\boldsymbol{\Theta}_2\tilde{\boldsymbol{g}}_k + \mathbf{H}_1\boldsymbol{\Theta}_1\boldsymbol{g}_k)v_k - 1|^2 \\
&\quad + \sigma^2\boldsymbol{u}^H\boldsymbol{u} \\
&= \sum_{k\in\mathcal{K}} |\boldsymbol{\theta}_2^H \mathrm{diag}(\boldsymbol{u}^H\mathbf{H}_2)\mathbf{Q}\mathrm{diag}(\boldsymbol{g}_k v_k)\boldsymbol{\theta}_1^* \\
&\quad + \boldsymbol{\theta}_2^H \mathrm{diag}(\boldsymbol{u}^H\mathbf{H}_2)\tilde{\boldsymbol{g}}_k v_k + \boldsymbol{\theta}_1^H \mathrm{diag}(\boldsymbol{u}^H\mathbf{H}_1)\boldsymbol{g}_k v_k - 1|^2 \\
&\quad + \sigma^2\boldsymbol{u}^H\boldsymbol{u}. \qquad (8)
\end{aligned}$$

Hence, we can mathematically formulate the computation MSE minimization problem as follows:

$$\begin{aligned}
\mathcal{P}1\colon \underset{\boldsymbol{\theta}_1,\boldsymbol{\theta}_2,\boldsymbol{u},v_k}{\text{minimize}} \ & \zeta(\{v_k\}, \boldsymbol{\theta}_1, \boldsymbol{\theta}_2, \boldsymbol{u}) \\
\text{subject to } & |v_k|^2 \le P, \forall k \in \mathcal{K}, \\
& \boldsymbol{\theta}_\mu \in \mathcal{F}_\mu, \mu \in \{1,2\},
\end{aligned} \qquad (9)$$

where $\mathcal{F}_\mu \triangleq \{\boldsymbol{\theta}_\mu = [\exp(j\phi_{\mu,1}), \ldots, \exp(j\phi_{\mu,M_\mu})]^T, \phi_{\mu,m} \in [0, 2\pi], m \in \mathcal{M}_\mu\}$ is the feasible set of $\boldsymbol{\theta}_\mu$.

As we can see, it is challenging to optimally solve problem $\mathcal{P}1$ mainly due to the unit modulus constraints on the passive beamforming vector $\boldsymbol{\theta}_\mu$ at the RISs. Furthermore, the variables (i.e., $\{v_k\}$, $\boldsymbol{\theta}_1$, $\boldsymbol{\theta}_2$, and $\boldsymbol{u}$) are highly coupled in the objective function. To the best of our knowledge, there is still a lack of effective algorithms to tackle this non-convex problem.

III. Proposed DRIS Beamforming Design

In this section, we propose a novel DRIS beamforming design for addressing problem $\mathcal{P}1$ based on alternating optimization. In particular, we first optimize the transmit coefficients at the WDs via the Lagrange duality method with the fixed receive beamforming vector at the FC and the passive beamforming vectors at the RISs. Then the receive beamforming vector is updated given the transmit coefficients and passive beamforming vectors based on the first optimality condition. Finally, we optimize the passive beamforming vectors by exploiting the SDR and PDD methods [42].

A. Optimization of the Transmit Coefficients $\{v_k\}$

Under the given receive vector $\boldsymbol{u}$ at the FC and the passive beamforming vectors $\boldsymbol{\theta}_\mu$ at the RISs with $\mu \in \{1,2\}$, we can obtain the solution for $\{v_k\}$ by solving the following subproblem in sequence with $k \in \mathcal{K}$:

$$\begin{aligned}
\mathcal{P}2\colon \underset{v_k}{\text{minimize}} \ & |\boldsymbol{u}^H\boldsymbol{h}_k v_k - 1|^2 \\
\text{subject to } & |v_k|^2 \le P, \forall k \in \mathcal{K},
\end{aligned} \qquad (10)$$

where $\boldsymbol{h}_k = \mathbf{H}_2\boldsymbol{\Theta}_2\mathbf{Q}\boldsymbol{\Theta}_1\boldsymbol{g}_k + \mathbf{H}_2\boldsymbol{\Theta}_2\tilde{\boldsymbol{g}}_k + \mathbf{H}_1\boldsymbol{\Theta}_1\boldsymbol{g}_k$ denotes the combined channel vector between WD k and the FC. One can see that problem $\mathcal{P}2$ is a quadratic optimization problem with only one convex constraint, which can be solved by some toolboxes, e.g., CVX. In this work, we exploit the Lagrange duality method to address this problem to reveal more insights, which is concluded in Lemma 1.

Lemma 1: The optimal solution for problem $\mathcal{P}2$ is formulated as

$$v_k^\star = \frac{\boldsymbol{h}_k^H\boldsymbol{u}}{\boldsymbol{u}^H\boldsymbol{h}_k\boldsymbol{h}_k^H\boldsymbol{u} + \lambda_k^\star}, \qquad (11)$$

where $\lambda_k^\star$ is the optimal Lagrange multiplier for WD k associated with the transmit power constraint. If the term $\boldsymbol{u}^H\boldsymbol{h}_k\boldsymbol{h}_k^H\boldsymbol{u}$ is not zero and

$$\left|\frac{\boldsymbol{h}_k^H\boldsymbol{u}}{\boldsymbol{u}^H\boldsymbol{h}_k\boldsymbol{h}_k^H\boldsymbol{u}}\right|^2 \le P, \qquad (12)$$

then $\lambda_k^\star = 0$. Otherwise, we need to choose $\lambda^\star$ such that the following equation holds via the bisection method:

$$\left|\frac{\boldsymbol{h}_k^H\boldsymbol{u}}{\boldsymbol{u}^H\boldsymbol{h}_k\boldsymbol{h}_k^H\boldsymbol{u} + \lambda_k^\star}\right|^2 = P. \qquad (13)$$

The results of Lemma 1 can be derived by joint exploiting the classic Karush-Kuhn-Tucker (KKT) conditions and the bisection method, where the detailed proof is omitted here to save space. From Lemma 1, we can update v_k in two steps: Firstly, we choose the optimal Lagrange multiplier $\lambda^\star$ to be zero or via the bisection method according to (13); Secondly, $v_k^\star$ is calculated by substituting $\lambda^\star$ into (11).

B. Optimization of the Receive Beamforming Vector $\boldsymbol{u}$

While fixing $\{v_k\}$, $\boldsymbol{\theta}_1$ and $\boldsymbol{\theta}_2$, the subproblem with respect to $\boldsymbol{u}$ is formulated as

$$\mathcal{P}3\colon \underset{\boldsymbol{u}}{\text{minimize}} \ \sum_{k\in\mathcal{K}} |\boldsymbol{u}^H\boldsymbol{h}_k v_k - 1|^2 + \sigma^2\boldsymbol{u}^H\boldsymbol{u}. \qquad (14)$$

We can see that problem $\mathcal{P}3$ is an unconstrained convex problem. Hence, the optimal solution for $\boldsymbol{u}$ can be obtained by exploiting the first optimality condition, which is given by

$$\boldsymbol{u}^\star = \left(\sum_{k\in\mathcal{K}} |v_k|^2\boldsymbol{h}_k\boldsymbol{h}_k^H + \sigma^2\mathbf{I}\right)^{-1} \sum_{k\in\mathcal{K}} \boldsymbol{h}_k v_k. \qquad (15)$$

Note that the obtained receive beamforming vector $\boldsymbol{u}^\star$ has a sum-MMSE structure, which can better utilize the "interference" from different WDs as a beneficial factor [16].

C. Optimization of the Passive Beamforming Vector $\boldsymbol{\theta}_1$

With the fixed $\{v_k\}$, $\boldsymbol{u}$, and $\boldsymbol{\theta}_2$, since the equations $\boldsymbol{a}^H\boldsymbol{b}^* = \boldsymbol{b}^H\boldsymbol{a}^*$ and $\boldsymbol{b}^T\boldsymbol{a} = \boldsymbol{a}^T\boldsymbol{b}$ hold for any non-zeros complex vectors $\boldsymbol{a}$ and $\boldsymbol{b}$, we can equivalently formulate the following subproblem with respect to $\boldsymbol{\theta}_1$:

$$\begin{aligned}\mathcal{P}4\colon \underset{\boldsymbol{\theta}_1}{\text{minimize}}\ & \boldsymbol{\theta}_1^H\mathbf{A}_1\boldsymbol{\theta}_1 + \boldsymbol{\theta}_1^H\boldsymbol{b}_1 + \boldsymbol{b}_1^H\boldsymbol{\theta}_1 \\ \text{subject to}\ & \boldsymbol{\theta}_1 \in \mathcal{F}_1,\end{aligned} \tag{16}$$

where

$$\begin{aligned}\mathbf{A}_1 \triangleq & \sum_{k\in\mathcal{K}} (|v_k|^2 \text{diag}(\mathbf{u}^H\mathbf{H}_1)\mathbf{g}_k\mathbf{g}_k^H \text{diag}^H(\mathbf{u}^H\mathbf{H}_1) \\ & + (\boldsymbol{\theta}_2^H \text{diag}(\mathbf{u}^H\mathbf{H}_2)\mathbf{Q}\text{diag}(\mathbf{g}_k v_k))^T v_k^*\mathbf{g}_k^H \text{diag}^H(\mathbf{u}^H\mathbf{H}_1) \\ & + \text{diag}(\mathbf{u}^H\mathbf{H}_1)\mathbf{g}_k v_k (\boldsymbol{\theta}_2^H \text{diag}(\mathbf{u}^H\mathbf{H}_2)\mathbf{Q}\text{diag}(\mathbf{g}_k v_k))^* \\ & + (\boldsymbol{\theta}_2^H \text{diag}(\mathbf{u}^H\mathbf{H}_2)\mathbf{Q}\text{diag}(\mathbf{g}_k v_k))^T \\ & \times (\boldsymbol{\theta}_2^H \text{diag}(\mathbf{u}^H\mathbf{H}_2)\mathbf{Q}\text{diag}(\mathbf{g}_k v_k))^*,\end{aligned} \tag{17}$$

$\boldsymbol{b}_1 \triangleq \sum_{k\in\mathcal{K}} (\text{diag}(\boldsymbol{u}^H\mathbf{H}_1)\boldsymbol{g}_k v_k)(v_k^*\tilde{\boldsymbol{g}}_k^H \text{diag}^H(\boldsymbol{u}^H\mathbf{H}_2)\boldsymbol{\theta}_2 + (\boldsymbol{\theta}_2^H \text{diag}(\boldsymbol{u}^H\mathbf{H}_2)\mathbf{Q}\text{diag}(\boldsymbol{g}_k v_k))^T - 1)$. As we can see, problem $\mathcal{P}4$ is a quadratic problem with constant modulus constraints. To address such passive beamforming optimization problem for RISs, SDR is generally considered as one of effective methods in the literature [35]–[38]. Besides, there are some other alternating methods, e.g., PDD and Manifold optimization. As shown in [42], [47], [48], the PDD framework can generate very good system performance with convergence guarantee in the optimization of passive beamforming in RIS-assisted communication systems and hybrid beamforming in massive MIMO systems. Furthermore, Manifold optimization is a gradient-descent-like iterative method, which is less efficient than the optimization method with closed-form solutions [49]. Moreover, the closed-form solutions of primary variables can be obtained in the PDD framework. Hence, we propose two methods to address problem $\mathcal{P}4$ based on the techniques of SDR and PDD [42] in the following, respectively.

1) The SDR-based method: By defining $\mathbf{R} = \begin{bmatrix}\mathbf{A}_1 & \boldsymbol{b}_1 \\ \boldsymbol{b}_1^H & 0\end{bmatrix}$, $\bar{\boldsymbol{\theta}}_1 = [\boldsymbol{\theta}_1^T, 1]^T$, and $\bar{\boldsymbol{\Theta}}_1 = \bar{\boldsymbol{\theta}}_1\bar{\boldsymbol{\theta}}_1^H$, we can reformulate problem $\mathcal{P}4$ equivalently as follows:

$$\begin{aligned}\mathcal{P}5\colon \underset{\bar{\boldsymbol{\Theta}}_1}{\text{minimize}}\ & \text{Tr}(\mathbf{R}\bar{\boldsymbol{\Theta}}_1) \\ \text{subject to}\ & \bar{\boldsymbol{\Theta}}_1(m,m) = 1, m \in \mathcal{M}_1, \\ & \bar{\boldsymbol{\Theta}}_1 \succeq \mathbf{0},\ \text{rank}(\bar{\boldsymbol{\Theta}}_1) = 1.\end{aligned} \tag{18}$$

Note that the second and third constraints are due to the definition of $\bar{\boldsymbol{\Theta}}_1$. However, problem $\mathcal{P}5$ is still non-convex with the rank-one constraint. Hence, we can exploit SDR to remove this constraint and problem $\mathcal{P}5$ can be rewritten as a convex semidefinite program (SDP), which can be optimally solved by exploiting some toolboxes, i.e., CVX.

However, we have to emphasize that the solution obtained by solving the relaxed problem of $\mathcal{P}5$ does not generally satisfy the rank-one constraint, which implies that this solution is only a lower bound of $\mathcal{P}5$. To tackle this issue, we employ the random-generalization-based method in [50], which can be briefly summarized in the following three steps: 1) firstly, we randomly generalize a vector $\boldsymbol{r} \in \mathbb{C}^{(M_1+1)\times 1}$ with distribution $\mathcal{CN}(\mathbf{0}, \mathbf{I})$ and set $\bar{\boldsymbol{\theta}}_1 = \boldsymbol{\Lambda}_1^H\mathbf{D}^{1/2}\boldsymbol{r}$, where $\bar{\boldsymbol{\Theta}}_1 = \boldsymbol{\Lambda}_1^H\mathbf{D}\boldsymbol{\Lambda}$ denotes the eigenvalue decomposition of $\bar{\boldsymbol{\Theta}}_1$; secondly, we choose the best $\bar{\boldsymbol{\theta}}_1$ among different values of $\boldsymbol{r}$ to minimize objective function value of problem $\mathcal{P}5$; finally, we can obtain the suboptimal solution of $\boldsymbol{\theta}_1$ by $\boldsymbol{\theta}_1 = \exp(j\arg([\bar{\boldsymbol{\theta}}_1/\bar{\boldsymbol{\theta}}_1(M_1+1)](1:M_1)))$, where $\arg(\boldsymbol{x})$ and $[\boldsymbol{x}](1:M_1)$ denote the angle vector of $\boldsymbol{x}$ and the vector containing the first M_1 elements of $\boldsymbol{x}$, respectively. The above method is proven to be efficient with a $\frac{\pi}{4}$–approximation of the optimal objective value of problem $\mathcal{P}5$ [51].

2) The PDD-based method: By introducing an auxiliary variable $\boldsymbol{f}_1 \in \mathbb{C}^{M_1\times 1}$, which satisfies $\boldsymbol{\theta}_1 = \boldsymbol{f}_1$, we can equivalently rewrite problem $\mathcal{P}4$ as follows:

$$\begin{aligned}\mathcal{P}6\colon \underset{\boldsymbol{\theta}_1,\boldsymbol{f}_1}{\text{minimize}}\ & \boldsymbol{\theta}_1^H\mathbf{A}_1\boldsymbol{\theta}_1 + \boldsymbol{\theta}_1^H\boldsymbol{b}_1 + \boldsymbol{b}_1^H\boldsymbol{\theta}_1 \\ \text{subject to}\ & \boldsymbol{\theta}_1 = \boldsymbol{f}_1,\ \boldsymbol{f}_1 \in \mathcal{F}_1.\end{aligned} \tag{19}$$

To solve problem $\mathcal{P}6$, inspired by [42], we consider a double-loop PDD-based method, where we exploit the BCD approach to alternatively optimize the primal variables in the inner loop, while in the outer loop, we update the dual variables and the penalty parameter. Firstly, we formulate the corresponding augmented Lagrangian problem of $\mathcal{P}6$ as follows:

$$\begin{aligned}\mathcal{P}7\colon \underset{\boldsymbol{\theta}_1,\boldsymbol{f}_1}{\text{minimize}}\ & \boldsymbol{\theta}_1^H\mathbf{A}_1\boldsymbol{\theta}_1 + \boldsymbol{\theta}_1^H\boldsymbol{b}_1 + \boldsymbol{b}_1^H\boldsymbol{\theta}_1 \\ & + \frac{1}{2\rho}\|\boldsymbol{\theta}_1 - \boldsymbol{f}_1 + \rho\boldsymbol{z}_1\|^2 \\ \text{subject to}\ & \boldsymbol{f}_1 \in \mathcal{F}_1,\ \|\boldsymbol{\theta}_1\|^2 \le M_1,\end{aligned} \tag{20}$$

where ρ denotes the penalty parameter and $\boldsymbol{z}_1 \in \mathbb{C}^{M_1\times 1}$ is the dual variable associated with the first constraint in problem $\mathcal{P}6$. Note that adding the second constraint $\|\boldsymbol{\theta}_1\|^2 \le M_1$ is mainly due to $|\boldsymbol{\theta}_1(m)| \le 1$, which can restrict the search space of problem $\mathcal{P}7$ and accelerate the convergence.

In the following, we optimize the primal variables, i.e., $\boldsymbol{\theta}_1$ and $\boldsymbol{f}_1$, in an alternating manner. While fixing $\boldsymbol{f}_1$, the subproblem with respect to $\boldsymbol{\theta}_1$ is given by

$$\begin{aligned}\mathcal{P}8\colon \underset{\boldsymbol{\theta}_1}{\text{minimize}}\ & \boldsymbol{\theta}_1^H\mathbf{A}_1\boldsymbol{\theta}_1 + \boldsymbol{\theta}_1^H\boldsymbol{b}_1 + \boldsymbol{b}_1^H\boldsymbol{\theta}_1 \\ & + \frac{1}{2\rho}\|\boldsymbol{\theta}_1 - \boldsymbol{f}_1 + \rho\boldsymbol{z}_1\|^2 \\ \text{subject to}\ & \|\boldsymbol{\theta}_1\|^2 \le M_1.\end{aligned} \tag{21}$$

One can see that, problem $\mathcal{P}8$ is a quadratic and convex problem, whose solution can be obtained by exploiting the first order optimality as follows:

$$\boldsymbol{\theta}_1^\star = \begin{cases} (2\rho\mathbf{A}_1 + \mathbf{I})^{-1}(\boldsymbol{f}_1 - \rho\boldsymbol{z}_1 - 2\rho\boldsymbol{b}_1), \\ \text{if } \|(2\rho\mathbf{A}_1 + \mathbf{I})^{-1}(\boldsymbol{f}_1 - \rho\boldsymbol{z}_1 - 2\rho\boldsymbol{b}_1)\|^2 \le M_1, \\ \dfrac{(2\rho\mathbf{A}_1 + \mathbf{I})^{-1}(\boldsymbol{f}_1 - \rho\boldsymbol{z}_1 - 2\rho\boldsymbol{b}_1)}{\sqrt{\|(2\rho\mathbf{A}_1 + \mathbf{I})^{-1}(\boldsymbol{f}_1 - \rho\boldsymbol{z}_1 - 2\rho\boldsymbol{b}_1)\|^2/M_1}}, \\ \text{otherwise.}\end{cases} \tag{22}$$

Next, we update $\boldsymbol{f}$ with the fixed $\boldsymbol{\theta}_1$, which leads to the following subproblem:

$$\begin{aligned}\mathcal{P}9\colon \underset{\boldsymbol{f}_1}{\text{minimize}}\ & \|\boldsymbol{\theta}_1 - \boldsymbol{f}_1 + \rho\boldsymbol{z}_1\|^2 \\ \text{subject to}\ & \boldsymbol{f}_1 \in \mathcal{F}_1.\end{aligned} \tag{23}$$

Algorithm 1 The PDD-Based Method for Problem $\mathcal{P}4$

Initialize $\boldsymbol{\theta}_1$, $\boldsymbol{f}_1$, ρ, and $\boldsymbol{z}_1$ such that they meet all the constraints and set $\epsilon_{\text{in}} > 0$, $\epsilon_{\text{out}} > 0$;

Repeat

Inner loop:

Update $\boldsymbol{\theta}_1$ and $\boldsymbol{f}_1$ alternatively according to (22) and (24), until the decrease of the objective function in problem $\mathcal{P}7$ is less than ϵ_{in};

Outer loop:

Update $\boldsymbol{z}_1$ and ρ according to (25) and (26);

Until the constraint violation $\|\boldsymbol{\theta}_1 - \boldsymbol{f}_1\|_\infty$ is below ϵ_{out}.

According to the definition of the feasible set $\mathcal{F}_1$, the elements of $\boldsymbol{f}_1$ are all separated in the constraint and the objective function of $\mathcal{P}9$. Hence, we can readily obtain the solution for $\boldsymbol{f}_1(m)$ as follows:

$$\boldsymbol{f}_1(m)^\star = \frac{\boldsymbol{\theta}_1(m) + \rho \boldsymbol{z}_1(m)}{|\boldsymbol{\theta}_1(m) + \rho \boldsymbol{z}_1(m)|}, m \in \mathcal{M}_1. \tag{24}$$

Finally, in the outer loop, we update the dual variable $\boldsymbol{z}_1$ and the penalty parameter ρ according to the following equations

$$\boldsymbol{z}_1 = \boldsymbol{z}_1 + \frac{1}{\rho}(\boldsymbol{\theta}_1 - \boldsymbol{f}_1), \tag{25}$$

$$\rho = \eta \rho, \tag{26}$$

where $\eta < 1$ is a positive constant to increase the value of the penalty term $\frac{1}{2\rho}\|\boldsymbol{f}_1 - \boldsymbol{\theta}_1 + \rho \boldsymbol{z}_1\|^2$ in the outer loop. The proposed PDD-based method for problem $\mathcal{P}4$ is summarized in Algorithm 1. According to [42], the convergence of this PDD-based method applied to problem $\mathcal{P}4$ is guaranteed. Note that as the penalty parameter decreases in each outer loop, the constraint violation, defined as the infinite norm of $\boldsymbol{f}_1 - \boldsymbol{\theta}_1$, i.e., $\|\boldsymbol{f}_1 - \boldsymbol{\theta}_1\|_\infty$, must be below a given threshold at any limit points generated by Algorithm 1.

D. Optimization of the Passive Beamforming Vector $\boldsymbol{\theta}_2$

With the fixed $\{v_k\}$, $\boldsymbol{u}$, and $\boldsymbol{\theta}_1$, the subproblem with respect to $\boldsymbol{\theta}_2$ is given by

$$\begin{aligned} \mathcal{P}10\colon \underset{\boldsymbol{\theta}_2}{\text{minimize}} \;& \boldsymbol{\theta}_2^H \mathbf{A}_2 \boldsymbol{\theta}_2 + \boldsymbol{\theta}_2^H \boldsymbol{b}_2 + \boldsymbol{b}_2^H \boldsymbol{\theta}_2 \\ \text{subject to } & \boldsymbol{\theta}_2 \in \mathcal{F}_2, \end{aligned} \tag{27}$$

where

$$\begin{aligned} \mathbf{A}_2 \triangleq & \sum_{k \in \mathcal{K}} \text{diag}(\boldsymbol{u}^H \mathbf{H}_2) \mathbf{Q} \text{diag}(\boldsymbol{g}_k v_k) \boldsymbol{\theta}_1^* \boldsymbol{\theta}_1^T \\ & \times \text{diag}^H(\boldsymbol{g}_k v_k) \mathbf{Q}^H \text{diag}^H(\boldsymbol{u}^H \mathbf{H}_2) \\ & + \text{diag}(\boldsymbol{u}^H \mathbf{H}_2) \mathbf{Q} \text{diag}(\boldsymbol{g}_k v_k) \boldsymbol{\theta}_1^* v_k^* \tilde{\boldsymbol{g}}_k^H \text{diag}^H(\boldsymbol{u}^H \mathbf{H}_2) \\ & + \text{diag}(\boldsymbol{u}^H \mathbf{H}_2) \tilde{\boldsymbol{g}}_k v_k \boldsymbol{\theta}_1^T \text{diag}^H(\boldsymbol{g}_k v_k) \mathbf{Q}^H \text{diag}^H(\boldsymbol{u}^H \mathbf{H}_2) \\ & + |v_k|^2 \text{diag}(\boldsymbol{u}^H \mathbf{H}_2) \tilde{\boldsymbol{g}}_k \tilde{\boldsymbol{g}}_k^H \text{diag}^H(\boldsymbol{u}^H \mathbf{H}_2)), \end{aligned} \tag{28}$$

$\boldsymbol{b}_2 \triangleq \sum_{k \in \mathcal{K}} (\text{diag}(\boldsymbol{u}^H \mathbf{H}_2) \mathbf{Q} \text{diag}(\boldsymbol{g}_k v_k) \boldsymbol{\theta}_1^* + \text{diag}(\boldsymbol{u}^H \mathbf{H}_2) \tilde{\boldsymbol{g}}_k v_k)(v_k^H \boldsymbol{g}_k^H \text{diag}^H(\boldsymbol{u}^H \mathbf{H}_1) \boldsymbol{\theta}_1 - 1)$. Hence, $\mathcal{P}10$ can also be solve by the SDR-based and PDD-based methods.

Algorithm 2 The DRIS-SDR/DRIS-PDD for Problem $\mathcal{P}1$

Initialize $\{v_k\}$, $\boldsymbol{u}$, $\boldsymbol{\theta}_1$, and $\boldsymbol{\theta}_2$ such that they meet all the constraints and set $\epsilon > 0$;

Repeat

Update v_k according to Lemma 1 in sequence;

Update $\boldsymbol{u}$ according to (15);

Update $\boldsymbol{\theta}_1$ by exploiting the SDR-based or PDD-based methods;

Update $\boldsymbol{\theta}_2$ by exploiting the SDR-based or PDD-based methods;

Until the decrease of the objective function value in problem $\mathcal{P}1$ is less than ϵ.

E. Complete Algorithm

The proposed DRIS beamforming design formulated as problem $\mathcal{P}1$ - namely DRIS-SDR or DRIS-PDD - is summarized in Algorithm 2. Note that the existing methods in the derivation cannot be applied directly, thus we propose some particularly efficient algorithms based on them. For instance, the new closed-form solutions for the transmit coefficients at the WDs and the receive beamforming vector at the FC need to be derived. Besides, we exploit the PDD framework only for updating the passive beamforming of RISs rather than directly solving problem $\mathcal{P}1$ since the closed-form solutions for other variables can be efficiently obtained.

The complexity of updating v_k is $\mathcal{O}(K(N + 2NM_2^2 + 2NM_1^2 + NM_1M_2 + NM_2 + 2NM_1))$, while the complexity of optimizing $\boldsymbol{u}$ is $\mathcal{O}(K(N^2 + N + 2NM_2^2 + 2NM_1^2 + NM_1M_2 + NM_2 + 2NM_1) + N^3)$. As shown in [20], the complexity of implementing the SDR-based method to update $\boldsymbol{\theta}_1$ and $\boldsymbol{\theta}_2$ is $\mathcal{O}((M_1+1)^{6.5})$ and $\mathcal{O}((M_2+1)^{6.5})$, respectively, while the complexity of implementing the PDD-based method to update $\boldsymbol{\theta}_1$ and $\boldsymbol{\theta}_2$ is $\mathcal{O}(I_i I_o (M_1^3 + M_1))$ and $\mathcal{O}(I_i I_o (M_2^3 + M_2))$, respectively, where I_i and I_o represent the maximum iteration numbers for the inner and outer loop, respectively. Besides, since the random-generalization-based method is applied in the DRIS-SDR algorithm, solving the SDP needs to be repeated several times, which will increase the complexity of the DRIS-SDR algorithm. Therefore, the proposed PDD-based method outperforms the SDR-based method in terms of the computational complexity. But the SDR-based method usually provides less computation MSE, which will be shown in the simulation results. Furthermore, the convergence of the proposed DRIS-SDR and DRIS-PDD algorithms is illustrated by the following theorem.

Theorem 1: Any limit point of the sequence generated by the DRIS-SDR and DRIS-PDD algorithms is guaranteed to converge to a stationary point of problem $\mathcal{P}1$.

Proof: See Appendix A. ■

IV. Comparison With the Single-RIS-Assisted AirComp Systems

In this section, we theoretically compare the computation MSE of the DRIS-assisted AirComp system to that of the SRIS-assisted AirComp system. Based on reasonable assumptions, we will show that the DRIS-assisted AirComp systems

achieve lower computation MSE than its SRIS-assisted AirComp counterpart.

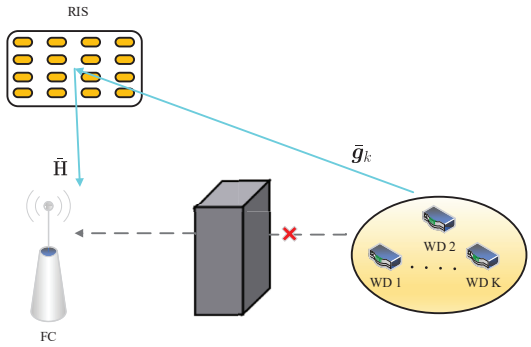

Fig. 2: SRIS-assisted AirComp system.

First, we introduce the general SRIS-assisted AirComp system model of Fig. 2. By comparing Fig. 2 to Fig. 1, we integrate RIS 1 and RIS 2 and formulate a single combined RIS with M passive reflecting elements, which is placed near the FC. Note that for fair comparison, we assume that the RISs are deployed symmetrically in the DRIS-assisted AirComp system as shown in Fig. 1, where the distance between the WDs and RIS 1 is the same as that between RIS 2 and the FC. Thus the distances of the WD–RIS 2 and RIS 1–FC links are also the same. Hence, there is no difference if we deploy the single combined RIS at the location of RIS 1 rather than that of RIS 2. The direct link between the WDs and the FC is unavailable due to obstacles and thus the WDs need to bypass the obstacles with the aid of the RIS. We would like to note that the transmit coefficient at WD k is fixed as $\bar{v}_k^\star$ in the DRIS-assisted and SRIS-assisted AirComp systems, which denotes the optimal transmit coefficient in the SRIS-assisted AirComp system. Therefore, we rewrite the computation MSE of the DRIS-assisted AirComp system as

$$\zeta(\{\bar{v}_k^\star\}) = \sum_{k\in\mathcal{K}} |\boldsymbol{u}^H(\mathbf{H}_2\boldsymbol{\Theta}_2\mathbf{Q}\boldsymbol{\Theta}_1\boldsymbol{g}_k + \mathbf{R}_{2,k}\boldsymbol{\theta}_2 + \mathbf{R}_{1,k}\boldsymbol{\theta}_1)\bar{v}_k^\star - 1|^2 + \sigma^2\boldsymbol{u}^H\boldsymbol{u}, \tag{29}$$

where $\mathbf{R}_{1,k} = \mathbf{H}_1\mathrm{diag}(\boldsymbol{g}_k)$ and $\mathbf{R}_{2,k} = \mathbf{H}_2\mathrm{diag}(\tilde{\boldsymbol{g}}_k)$. In the SRIS-assisted AirComp system as shown in Fig. 2, by denoting $\bar{\boldsymbol{g}}_k \in \mathbb{C}^{M\times 1}$, $\bar{\mathbf{H}} \in \mathbb{C}^{N\times M}$, $\bar{\boldsymbol{\Theta}} \in \mathbb{C}^{M\times M}$, and $\bar{\boldsymbol{u}} \in \mathbb{C}^{N\times 1}$ as the channel vectors from WD k to the RIS, the channel matrix from the RIS to the FC, the passive beamforming matrix at the RIS, and the receive beamforming vector at the FC, respectively, the received signal at the FC is given by

$$\bar{s} = \bar{\boldsymbol{u}}^H\left(\sum_{k\in\mathcal{K}} \bar{\mathbf{H}}\bar{\boldsymbol{\Theta}}\bar{\boldsymbol{g}}_k\bar{v}_k^\star s_k + \boldsymbol{n}\right). \tag{30}$$

Similarly, the computation MSE of the SRIS-assisted AirComp system is formulated as

$$\begin{aligned}\bar{\zeta}(\{\bar{v}_k^\star\}) &= \sum_{k\in\mathcal{K}} |\bar{\boldsymbol{u}}^H\bar{\mathbf{H}}\bar{\boldsymbol{\Theta}}\bar{\boldsymbol{g}}_k\bar{v}_k^\star - 1|^2 + \sigma^2\bar{\boldsymbol{u}}^H\bar{\boldsymbol{u}} \\ &= \sum_{k\in\mathcal{K}} |\bar{\boldsymbol{u}}^H\bar{\mathbf{R}}_k\bar{\boldsymbol{\theta}}\bar{v}_k^\star - 1|^2 + \sigma^2\bar{\boldsymbol{u}}^H\bar{\boldsymbol{u}},\end{aligned} \tag{31}$$

where $\bar{\mathbf{R}}_k = \bar{\mathbf{H}}\mathrm{diag}(\bar{\boldsymbol{g}}_k)$ and $\bar{\boldsymbol{\theta}} = \mathrm{diag}(\bar{\boldsymbol{\Theta}}^*)$.

To obtain more insights, we consider the following assumptions in our analysis.

***Assumption** 1:* In the SRIS-assisted AirComp system, we assume that $\bar{\mathbf{R}}_k = [\mathbf{R}_{1,k}, \mathbf{R}_{2,k}], \forall k \in \mathcal{K}$ and $\bar{\boldsymbol{\theta}} = [\boldsymbol{\theta}_2^T, \boldsymbol{\theta}_2^T]^T$ for any given channel realization.

***Assumption** 2:* We assume that the numbers of the antennas at the FC and the passive reflecting elements at the RISs are sufficiently large such that the combined channel vectors in the DRIS-assisted AirComp system are orthogonal, i.e.,

$$\frac{1}{N}\boldsymbol{h}_k^H\boldsymbol{h}_{k'} \approx 0, \forall k, k' \in \mathcal{K}, k \neq k'. \tag{32}$$

Similarly, the combined channel vectors in the SRIS-assisted AirComp system are also assumed to be orthogonal,

$$\frac{1}{N}\bar{\boldsymbol{h}}_k^H\bar{\boldsymbol{h}}_{k'} \approx 0, \forall k, k' \in \mathcal{K}, k \neq k', \tag{33}$$

where $\bar{\boldsymbol{h}}_k = \bar{\mathbf{H}}\bar{\boldsymbol{\Theta}}\bar{\boldsymbol{g}}_k = \bar{\mathbf{R}}_k\bar{\boldsymbol{\theta}}$.

Considering the symmetric deployment RISs in Fig. 1, the pathloss of cascaded single-reflection links $\mathbf{R}_{1,k}$ and $\mathbf{R}_{2,k}$ is the same due to their same cascaded distances. Similarly, the pathloss of the cascaded channel $\bar{\mathbf{R}}_k$ between the WDs and FC in Fig. 2 is also the same as those of $\mathbf{R}_{1,k}$ and $\mathbf{R}_{2,k}$. Besides, since we combine RIS 1 with RIS 2 to formulate a single RIS in Fig. 2, it is also reasonable in terms of structure to construct the cascaded channels and the passive beamforming vector in the SRIS-assisted AirComp system by stacking those in the DRIS-assisted AirComp system [39]. Furthermore, for sufficiently large numbers of antennas at the FC and passive reflecting elements at the RISs, the equivalent channels between the WDs and the FC tend to be orthogonal. Based on the law of large numbers (LLN), Assumption 2 is also reasonable [52]. To analyze the computation MSE of both SRIS-assisted and DRIS-assisted AirComp systems, we first rewrite their computation MSE based on the following lemma.

***Lemma** 2:* By applying the sum-MMSE receive beamforming at the FC, the computation MSE in the SRIS-assisted and DRIS-assisted AirComp systems, i.e., (29) and (31), can approximately be rewritten as

$$\bar{\zeta}(\{\bar{v}_k^\star\}) \approx K - \frac{1}{\sigma^2}\sum_{k\in\mathcal{K}}\left(|\bar{v}_k^\star|^2\bar{\boldsymbol{h}}_k^H\bar{\boldsymbol{h}}_k - \frac{|\bar{v}_k^\star|^4|\bar{\boldsymbol{h}}^H\bar{\boldsymbol{h}}_k|^2}{\sigma^2 + |\bar{v}_k^\star|^2\bar{\boldsymbol{h}}_k^H\bar{\boldsymbol{h}}_k}\right), \tag{34}$$

$$\zeta(\{\bar{v}_k^\star\}) \approx K - \frac{1}{\sigma^2}\sum_{k\in\mathcal{K}}\left(|\bar{v}_k^\star|^2\boldsymbol{h}_k^H\boldsymbol{h}_k - \frac{|\bar{v}_k^\star|^4|\boldsymbol{h}^H\boldsymbol{h}_k|^2}{\sigma^2 + |\bar{v}_k^\star|^2\boldsymbol{h}_k^H\boldsymbol{h}_k}\right), \tag{35}$$

respectively.

Proof: See Appendix B. ■

With the aid of Lemma 2, we simplify the computation MSE of the SRIS-assisted and DRIS-assisted AirComp systems to a more tractable form. Therefore, we can compare the computation MSE of the SRIS-assisted and DRIS-assisted AirComp systems, which is summarized in the following theorem.

***Theorem** 2:* With Assumption 1 and Lemma 2, the computation MSE of the DRIS-assisted AirComp system is less than that of the SRIS-assisted one, i.e., $\zeta(\{\bar{v}_k^\star\}) < \bar{\zeta}(\{\bar{v}_k^\star\})$.

Proof: See Appendix C. ■

Upon denoting the optimal transmit coefficients at the WDs in the DRIS-assisted AirComp system by $\{v_k^\star\}$, we have $\zeta(\{v_k^\star\}) \leq \zeta(\{\bar{v}_k^\star\}) < \bar{\zeta}(\{\bar{v}_k^\star\})$. Though the deployment of two RISs may lead to large pathloss, this large pathloss only exists in the double reflection links, which does not affect the single-reflection links and Assumption 1. Hence, the result of Theorem 2 still holds. Besides, from the proof of Theorem 2, the channel gain of double-reflection links with large pathloss is vital to ensure that the inequality of (51) holds. From the above derivation, we can infer that the deployment of two RISs provides the less computation MSE for the AirComp system by benefiting from more channel gain as compared with that of a single RIS with the same budget of passive beamforming elements, in the case where the direction link between the WDs and the FC is unavailable. This further strengthens the motivation of this paper.

V. Simulation Results

In this section, we evaluate the performance of the DRIS-SDR and DRIS-PDD beamforming algorithms designed for the proposed DRIS-assisted AirComp system in comparison to the following benchmark schemes.

- DRIS-BCD: In this scheme, we consider a BCD-type method to optimize the passive beamforming matrices of the RISs. In particular, we update the passive beamforming elements in sequence by exploiting the BCD method [20], while optimizing the transmit coefficients at the WDs and the receive beamforming vector at the FC based on Lemma 1 and (15).
- DRIS-MO: In this scheme, we consider a Manifold-optimization based method to update the passive beamforming matrices in [54].
- SRIS-PDD: In this scheme, we consider a SRIS-assisted AirComp system shown in Fig. 2. The transmit coefficients at the WDs and the receive beamforming vector at the FC are updated based on the Lagrange duality method and the first-order optimality condition, respectively. Then the passive beamforming matrix at the single RIS is optimized by exploiting PDD, which is similar to Algorithm 1.

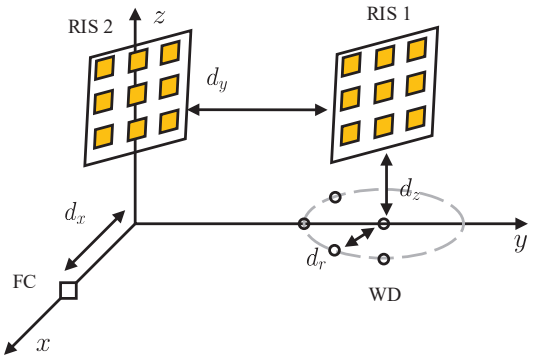

Fig. 3: The location setup of the FC, WDs, and RISs in the simulations.

In our experiments the path loss is defined as $L = C_0 \left(\frac{d}{D_0}\right)^{-\alpha}$, which depends on the distance. C_0, d, and α denote the reference path loss at $D_0 = 1$ meter, the distance, and the path loss exponent. Hence, we denote α_{W1}, α_{W2}, α_{RR}, α_{1F}, and α_{2F} as the path loss exponents for the links from the WDs to RIS 1, from WDs to RIS 2, from RIS 1 to RIS 2, from RIS 1 to the FC, and from RIS 2 to the FC, respectively. Considering the fact that RIS 1 and RIS 2 are respectively deployed near the WDs and the FC to assist the computation, the path losses from the WDs to RIS 2 and from RIS 1 to the FC are assumed to be larger than those from the WDs to RIS 1 and from RIS 2 to the FC, respectively. Then we choose $\alpha_{W1} = \alpha_{2F} = 2.2$, $\alpha_{W2} = \alpha_{1F} = 3.4$, and $\alpha_{RR} = 3$. As shown in Fig. 3, a three-dimensional system is considered in our simulation results, where the FC and the RISs are respectively deployed on the x-axis and $y-z$ plane. As illustrated in Section II, the FC is equipped with a ULA, while the RISs employ the UPA. Without loss of generality, we set the numbers of elements at the RISs along the y-axis to be 4, i.e., $M_{y,1} = M_{y,2} = 4$. The reference antenna at the FC and the reference passive beamforming elements at RIS 1 and RIS 2 are deployed at $(d_x = 1\text{ m}, 0, 0)$, $(0, d_y = 50\text{ m}, d_z = 1\text{ m})$, and $(0, 0, d_z = 1\text{ m})$, respectively. By choosing $(0, d_y = 50\text{ m}, 0)$ as a circle center, we uniformly deploy the WDs on the circle with $d_r = 3$ m. The signal-to-noise-ratio (SNR) is defined as SNR $= \frac{P}{\sigma^2}$. The carrier frequency is assumed to be 6 GHz with the wavelength of 0.05 m. The spacing of the antennas/elements is half a wavelength. Unless otherwise specified, we consider the following system parameters: $M = 64$, $M_1 = 32$, $M_2 = 32$, $N = 32$, $K = 64$, $\sigma^2 = -60\,\text{dBm}$, $C_0 = -30\,\text{dB}$, $\beta_{WR_1} = \beta_{R_2F} = 3\,\text{dB}$, $\beta_{WR_2} = \beta_{R_1F} = -3\,\text{dB}$, $\beta_{RR} = 2\,\text{dB}$, $\epsilon = \epsilon_{\text{in}} = 10^{-4}$, $\rho = 1$, and $\epsilon_{\text{out}} = 10^{-6}$.

A. Convergence

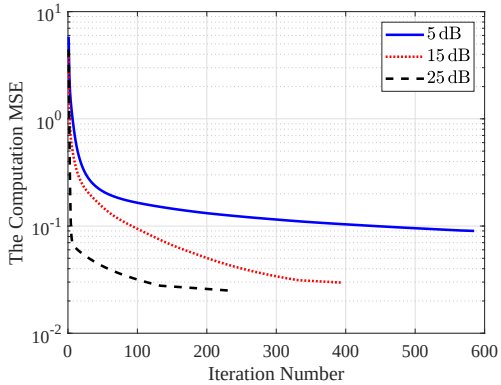

Fig. 4: The convergence of the DRIS-SDR algorithm with SNR $= 5\,\text{dB}$, $15\,\text{dB}$, and $25\,\text{dB}$.

The convergence behaviors of the DRIS-SDR and DRIS-PDD algorithms are shown in Figs. 4 and 5, respectively. Observe in Fig. 4 that the computation MSE of the DRIS-assisted AirComp system monotonically converges to a stationary point after a few number of iterations when we apply the DRIS-SDR algorithm to problem $\mathcal{P}1$ with SNR $= 5\,\text{dB}$, $15\,\text{dB}$,

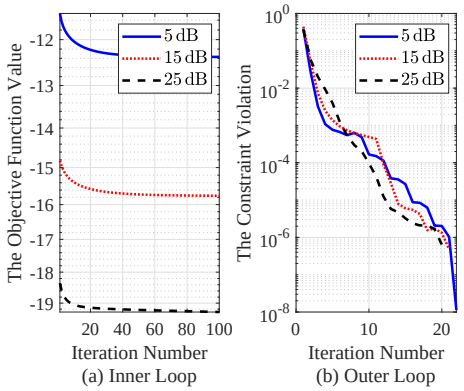

Fig. 5: The convergence of the DRIS-PDD algorithm with SNR $= 5\,\text{dB}$, $15\,\text{dB}$, and $25\,\text{dB}$.

and $25\,\text{dB}$. Furthermore, the DRIS-SDR algorithm converges faster in the low-SNR region. By exploiting the DRIS-PDD algorithm, we can also see from Fig. 5 that the objective function value of problem $\mathcal{P}7$ converges to a stationary point in the inner loop and the constraint violation vanishes in the outer loop under different SNRs. The unit modulus constraints are satisfied eventually. These simulation results further verify Theorem 1.

B. Impact of the Number of WDs

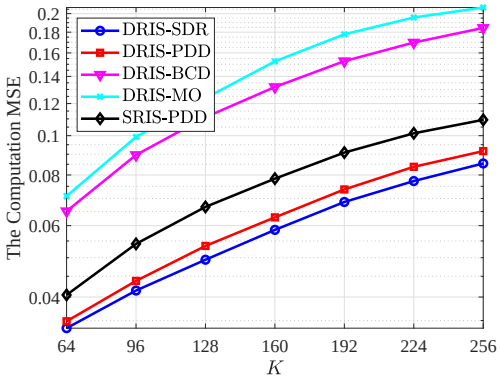

Fig. 6: The computation MSE versus K with SNR $= 15\,\text{dB}$.

The computation MSE versus K is shown in Fig. 6 with SNR $= 15$ dB. As we can see, the computation MSE of all the considered schemes becomes worse as K increases, due to the fact that some WDs with terrible transmit condition may significantly affect the computational accuracy. Moreover, it is more challenging to design the passive beamforming matrices at the RISs and the receive beamforming vector at the FC to enable the AirComp of more WDs, which is at the cost of degrading computational accuracy. The DRIS-SDR algorithm shows the best computation MSE and outperforms the DRIS-PDD algorithm by a small margin. This is due to the fact that the DRIS-SDR algorithm can optimally solve problem $\mathcal{P}5$ and generate a feasible solution with a $\frac{\pi}{4}$-approximation of the optimal objective value, while the DRIS-PDD algorithm usually obtains a suboptimal solution of problem $\mathcal{P}6$. However, as it will become explicit from the complexity analysis of Section III-E, the outstanding performance of the DRIS-SDR algorithm is attained at the cost of high complexity. Furthermore, observe that both our proposed algorithms outperform the DRIS-BCD algorithm with an increasing gap¿ This is because the latter updates the diagonal elements of passive beamforming matrices one by one, which may result in a suboptimal solution. Additionally, since the DRIS-MO algorithm may not exploit the spatial degree of freedom, it shows higher computation MSE than that of the DRIS-BCD algorithm. Though the SRIS-PDD algorithm applies the similar method, it achieves the worse computation performance as compared to the DRIS-PDD algorithm. This coincides with our discussion in Section IV. The SRIS-PDD algorithm still outperforms the DRIS-BCD and DRIS-MO algorithms, which means the benefits of the chosen method can overcome the drawbacks of system model.

C. Impact of the Number of Receive Antennas at the FC

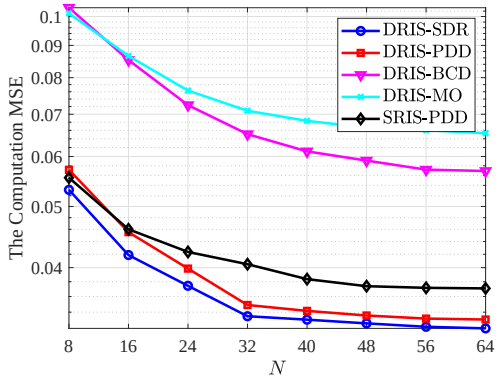

Fig. 7: The computation MSE versus N with SNR $= 15\,\text{dB}$.

The computation MSE versus N is shown in Fig. 7 under different setups. As we can see, the computation MSE of our proposed algorithms, the DRIS-BCD algorithm, the DRIS-MO algorithm, and the SRIS-PDD algorithm decreases significantly and converges to a limit point as N increases. This is due to the rich spatial degree of freedom brought by the antenna array at the FC and the fact that the computation performance of the algorithms tends to be saturated. In particular, the proposed DRIS-SDR and DRIS-PDD algorithms outperform the DRIS-BCD and DRIS-MO algorithms, which is mainly due to the fact that our proposed algorithms can offer a better solution for DRIS-assisted AirComp systems compared to the heuristic algorithms based on the BCD method and Manifold optimization by exploiting the structure of the problem $\mathcal{P}1$. Furthermore, we can observe that the SRIS-PDD algorithm shows less computation MSE than the DRIS-PDD algorithm when $N < 16$, while the opposite holds when $N \geq 16$. This coincides with our analysis and Assumption 2 in Section IV. Without the assumption of sufficiently large numbers of receive antennas and reflecting elements, the DRIS-PDD algorithm may not perform well. Similarly, the DRIS-MO algorithm outperforms the DRIS-BCD algorithm when N is

small, but shows worse performance when N becomes large, due to fact that the latter does not work well with limited spatial degree. Furthermore, it is clear that our proposed algorithms outperform other considered schemes when $N \geq 16$, which verifies the effectiveness of the proposed beamforming design for the DRIS-assisted AirComp system.

D. Impact of SNR

Fig. 8 compares the computation MSE versus the SNR among the considered schemes. One can see that, the computation MSE of the considered schemes decreases monotonically as SNR increases. It can be observed that the DRIS-MO algorithm outperforms the DRIS-BCD and SRIS-PDD algorithms when SNR $< 5\,$dB due to the deployment of two RISs. However, as SNR increases, the SRIS-PDD algorithm achieves less computation MSE than that achieved by the DRIS-BCD and DRIS-MO algorithms, which shows its advantages of optimizing the passive beamforming matrix at the RIS. Similarly, the cross point between the DRIS-BCD and DRIS-MO algorithms is mainly due to the latter's advantages of exploiting channel gain in the low-SNR region. Moreover, our proposed algorithms still outperform the SRIS-PDD algorithm. The gaps between the SRIS-PDD algorithm and our proposed DRIS-SDR and DRIS-PDD algorithms are roughly $5\,$dB and $2\,$dB, respectively.

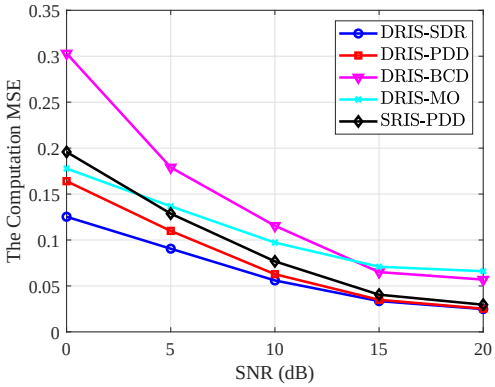

Fig. 8: The computation MSE versus SNR.

E. Impact of the Number of Reflecting Elements at the RISs

Fig. 9 compares the computation MSE versus the total budget of passive beamforming elements at the RISs with $M_1 = M/2$ and SNR $= 15\,$dB. It is shown that the computation MSE of all the considered schemes decreases significantly due to the increasing spatial degrees. The proposed DRIS-PDD algorithm achieves less computation MSE than the DRIS-BCD, DRIS-MO, and SRIS-PDD algorithms when $M \geq 16$. Besides, when $M < 8$, the SRIS-PDD algorithm outperforms the DRIS-PDD algorithm due to the same reason illustrated in Fig. 7 of the manuscript. Furthermore, the DRIS-SDR algorithm still generates the least computation MSE among all the considered schemes.

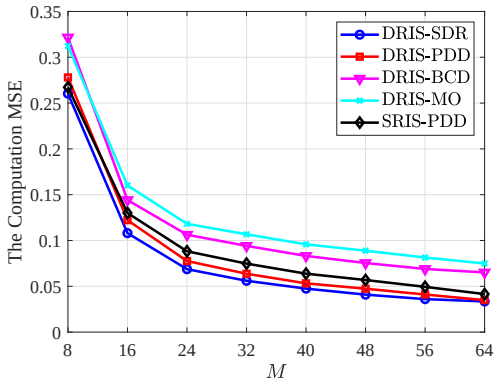

Fig. 9: The computation MSE versus M with $M_1 = M/2$ and SNR $= 15\,$dB.

VI. Conclusion

The family of DRIS-assisted AirComp systems was investigated, where the direct link between the FC and the WDs may be unavailable due to obstacles. To minimize the computation MSE, we proposed the DRIS-SDR and DRIS-PDD algorithms to jointly optimize the transmit coefficients at the WDs, the receive beamforming vector at the FC, and the passive beamforming matrices at the RISs. Specifically, we developed two approaches based on the SDR and PDD techniques to update the passive beamforming matrices. The complexity and convergence of the proposed algorithms were analyzed. To gain more insights, under some reasonable assumptions, we mathematically proved that the computation MSE achieved by the DRIS-assisted AirComp system is less than that achieved by the SRIS-assisted AirComp system. Simulation results showed that our proposed algorithms can provide the outstanding computation performance and outperform the considered benchmark schemes. Hence, this paper offers promising beamforming design algorithms for the DRIS-assisted AirComp system.

Appendix A
Proof of Theorem 1

We commence by observing that the feasible sets of the considered variables ($\{v_k\}$, $\boldsymbol{u}$, $\boldsymbol{\theta}_1$, and $\boldsymbol{\theta}_2$) are all compact, which means that problem $\mathcal{P}1$ over their Cartesian product set is bounded. Hence, the sequence generated by the DRIS-SDR and DRIS-PDD algorithms is compact and bounded such that there must exists a limit point of our proposed algorithms.

Secondly, we observe from the procedures in Algorithm 2 that the considered objective functions of problems $\mathcal{P}2$, $\mathcal{P}3$, $\mathcal{P}4$, and $\mathcal{P}6$ are all equivalent to that of problem $\mathcal{P}1$. Thus the objective function of $\mathcal{P}1$ is lower bounded at each iteration.

Thirdly, we show that the sequence generated by the DRIS-SDR/DRIS-PDD algorithm is non-increasing. Under given $\boldsymbol{u}_r$, $\boldsymbol{\theta}_{1,r}$, and $\boldsymbol{\theta}_{2,r}$, since $\{v_{k,r+1}\}$ is updated according to Lemma 1 based on the KKT conditions and the bisection method, we have

$$\zeta(\{v_{k,r+1}\}, \boldsymbol{\theta}_{1,r}, \boldsymbol{\theta}_{2,r}, \boldsymbol{u}_r) \leq \zeta(\{v_{k,r}\}, \boldsymbol{\theta}_{1,r}, \boldsymbol{\theta}_{2,r}, \boldsymbol{u}_r). \quad (36)$$

We can have the similar result as follows due to the fact that $\boldsymbol{u}_{r+1}$ is updated with fixed $\{v_{k,r}\}$, $\boldsymbol{\theta}_{1,r}$, and $\boldsymbol{\theta}_{2,r}$ based on the first-order optimality condition:

$$\zeta(\{v_{k,r}\}, \boldsymbol{\theta}_{1,r}, \boldsymbol{\theta}_{2,r}, \boldsymbol{u}_{r+1}) \leq \zeta(\{v_{k,r}\}, \boldsymbol{\theta}_{1,r}, \boldsymbol{\theta}_{2,r}, \boldsymbol{u}_{r}). \quad (37)$$

By exploiting the concept of SDR and the random-generalization-based method, a solution of problem $\mathcal{P}5$ with a $\frac{\pi}{4}$–approximation of the optimal objective value can be obtained. Furthermore, the PDD-based method can be proven to converge to a stationary point of problem $\mathcal{P}4$. Therefore, the following inequalities holds:

$$\zeta(\{v_{k,r}\}, \boldsymbol{\theta}_{1,r+1}, \boldsymbol{\theta}_{2,r}, \boldsymbol{u}_{r}) \leq \zeta(\{v_{k,r}\}, \boldsymbol{\theta}_{1,r}, \boldsymbol{\theta}_{2,r}, \boldsymbol{u}_{r}), \quad (38)$$

$$\zeta(\{v_{k,r}\}, \boldsymbol{\theta}_{1,r}, \boldsymbol{\theta}_{2,r+1}, \boldsymbol{u}_{r}) \leq \zeta(\{v_{k,r}\}, \boldsymbol{\theta}_{1,r}, \boldsymbol{\theta}_{2,r}, \boldsymbol{u}_{r}). \quad (39)$$

By combining (36)-(39), the objective function value of problem $\mathcal{P}1$ is lower bounded by zero and non-increasing at each iteration. The result follows immediately.

Appendix B
Proof of Lemma 2

According to (31) and the derivation of the receive beamforming at the FC in Section III, the sum-MMSE receive beamforming to minimize the computation MSE in the SRIS-assisted AirComp system is given by

$$\bar{\boldsymbol{u}}^{\star} = \left(\sum_{k\in\mathcal{K}} |\bar{v}_k^{\star}|^2 \bar{\boldsymbol{h}}_k \bar{\boldsymbol{h}}_k^H + \sigma^2 \mathbf{I}\right)^{-1} \sum_{k\in\mathcal{K}} \bar{\boldsymbol{h}}_k \bar{v}_k^{\star}. \quad (40)$$

By substituting $\bar{\boldsymbol{u}}^{*}$ into (31), we have

$$\begin{aligned}
&\bar{\zeta}(\{\bar{v}_k^{\star}\}) \\
&= K + (\bar{\boldsymbol{u}}^{\star})^H \left(\sum_{k\in\mathcal{K}} |\bar{v}_k^{\star}|^2 \bar{\boldsymbol{h}}_k \bar{\boldsymbol{h}}_k^H + \sigma^2 \mathbf{I}\right) \bar{\boldsymbol{u}}^{*} \\
&\quad - (\bar{\boldsymbol{u}}^{*})^H \sum_{k\in\mathcal{K}} \bar{\boldsymbol{h}}_k \bar{v}_k^{\star} - \sum_{k\in\mathcal{K}} (\bar{v}_k^{\star})^{*} \bar{\boldsymbol{h}}_k^H \bar{\boldsymbol{u}}^{*} \\
&= K - \left(\sum_{k\in\mathcal{K}} (\bar{v}_k^{\star})^{*} \bar{\boldsymbol{h}}_k^H\right) \left(\sum_{k\in\mathcal{K}} |\bar{v}_k^{\star}|^2 \bar{\boldsymbol{h}}_k \bar{\boldsymbol{h}}_k^H + \sigma^2 \mathbf{I}\right)^{-1} \\
&\quad \times \left(\sum_{k\in\mathcal{K}} \bar{\boldsymbol{h}}_k \bar{v}_k^{\star}\right). \quad (41)
\end{aligned}$$

As we can see, the main challenge in analyzing the computation MSE is due to the intractable term $\left(\sum_{k\in\mathcal{K}} |\bar{v}_k^{\star}|^2 \bar{\boldsymbol{h}}_k \bar{\boldsymbol{h}}_k^H + \sigma^2 \mathbf{I}\right)^{-1}$. To simplify this term, we first define a matrix sequence as follows:

$$\mathbf{D}_n = \sum_{k=1}^{n} |\bar{v}_k^{\star}|^2 \bar{\boldsymbol{h}}_k \bar{\boldsymbol{h}}_k^H + \sigma^2 \mathbf{I}, \forall n \in \mathcal{K}. \quad (42)$$

Hence, the above matrix sequence satisfies $\mathbf{D}_n = \mathbf{D}_{n-1} + |\bar{v}_n^{\star}|^2 \bar{\boldsymbol{h}}_n \bar{\boldsymbol{h}}_n^H$ and $\mathbf{D}_K = \sum_{k\in\mathcal{K}} |\bar{v}_k^{\star}|^2 \bar{\boldsymbol{h}}_k \bar{\boldsymbol{h}}_k^H + \sigma^2 \mathbf{I}$. By exploiting the Sherman-Morrison formula [53], we can derive the inverse of $\mathbf{D}_n$ as follows:

$$\mathbf{D}_n^{-1} = \mathbf{D}_{n-1}^{-1} - \frac{\mathbf{D}_{n-1}^{-1} |\bar{v}_n^{\star}|^2 \bar{\boldsymbol{h}}_n \bar{\boldsymbol{h}}_n^H \mathbf{D}_{n-1}^{-1}}{1 + |\bar{v}_n^{\star}|^2 \bar{\boldsymbol{h}}_n^H \mathbf{D}_{n-1}^{-1} \bar{\boldsymbol{h}}_n}. \quad (43)$$

Let n be 1, then we have

$$\begin{aligned}
\mathbf{D}_1^{-1} &= \frac{1}{\sigma^2}\mathbf{I} - \frac{1}{\sigma^4} \frac{|\bar{v}_1^{\star}|^2 \bar{\boldsymbol{h}}_1 \bar{\boldsymbol{h}}_1^H}{1 + |\bar{v}_1^{\star}|^2 \bar{\boldsymbol{h}}_1^H \bar{\boldsymbol{h}}_1 / \sigma^2} \\
&= \frac{1}{\sigma^2} \left(\mathbf{I} - \frac{|\bar{v}_1^{\star}|^2 \bar{\boldsymbol{h}}_1 \bar{\boldsymbol{h}}_1^H}{\sigma^2 + |\bar{v}_1^{\star}|^2 \bar{\boldsymbol{h}}_1^H \bar{\boldsymbol{h}}_1}\right). \quad (44)
\end{aligned}$$

Similarly, we can derive $\mathbf{D}_2^{-1}$ as follows:

$$\begin{aligned}
&\mathbf{D}_2^{-1} \\
&= \mathbf{D}_1^{-1} - \frac{\mathbf{D}_1^{-1} |\bar{v}_2^{\star}|^2 \bar{\boldsymbol{h}}_2 \bar{\boldsymbol{h}}_2^H \mathbf{D}_1^{-1}}{1 + |\bar{v}_2^{\star}|^2 \bar{\boldsymbol{h}}_2^H \mathbf{D}_1^{-1} \bar{\boldsymbol{h}}_2} \\
&\approx \frac{1}{\sigma^2} \left(\mathbf{I} - \frac{|\bar{v}_1^{\star}|^2 \bar{\boldsymbol{h}}_1 \bar{\boldsymbol{h}}_1^H}{\sigma^2 + |\bar{v}_1^{\star}|^2 \bar{\boldsymbol{h}}_1^H \bar{\boldsymbol{h}}_1}\right) - \frac{1}{\sigma^4} \frac{|\bar{v}_2^{\star}|^2 \bar{\boldsymbol{h}}_2 \bar{\boldsymbol{h}}_2^H}{1 + |\bar{v}_2^{\star}|^2 \bar{\boldsymbol{h}}_2^H \bar{\boldsymbol{h}}_2 / \sigma^2} \\
&= \frac{1}{\sigma^2} \left(\mathbf{I} - \frac{|\bar{v}_1^{\star}|^2 \bar{\boldsymbol{h}}_1 \bar{\boldsymbol{h}}_1^H}{\sigma^2 + |\bar{v}_1^{\star}|^2 \bar{\boldsymbol{h}}_1^H \bar{\boldsymbol{h}}_1} - \frac{|\bar{v}_2^{\star}|^2 \bar{\boldsymbol{h}}_2 \bar{\boldsymbol{h}}_2^H}{\sigma^2 + |\bar{v}_2^{\star}|^2 \bar{\boldsymbol{h}}_2^H \bar{\boldsymbol{h}}_2}\right), \quad (45)
\end{aligned}$$

where the approximation comes from Assumption 2. Hence, we can calculate $\mathbf{D}_K^{-1}$ recursively:

$$\mathbf{D}_K^{-1} \approx \frac{1}{\sigma^2} \left(\mathbf{I} - \sum_{k\in\mathcal{K}} \frac{|\bar{v}_k^{\star}|^2 \bar{\boldsymbol{h}}_k \bar{\boldsymbol{h}}_k^H}{\sigma^2 + |\bar{v}_k^{\star}|^2 \bar{\boldsymbol{h}}_k^H \bar{\boldsymbol{h}}_k}\right). \quad (46)$$

By substituting (46) into (41), we obtain

$$\begin{aligned}
&\bar{\zeta}(\{\bar{v}_k^{\star}\}) \\
&\approx K - \frac{1}{\sigma^2} \left(\sum_{k\in\mathcal{K}} (\bar{v}_k^{\star})^{*} \bar{\boldsymbol{h}}_k^H\right) \\
&\quad \times \left(\mathbf{I} - \sum_{k\in\mathcal{K}} \frac{|\bar{v}_k^{\star}|^2 \bar{\boldsymbol{h}}_k \bar{\boldsymbol{h}}_k^H}{\sigma^2 + |\bar{v}_k^{\star}|^2 \bar{\boldsymbol{h}}_k^H \bar{\boldsymbol{h}}_k}\right) \left(\sum_{k\in\mathcal{K}} \bar{\boldsymbol{h}}_k \bar{v}_k^{\star}\right) \\
&\approx K - \frac{1}{\sigma^2} \sum_{k\in\mathcal{K}} \left(|\bar{v}_k^{\star}|^2 \bar{\boldsymbol{h}}_k^H \bar{\boldsymbol{h}}_k - \frac{|\bar{v}_k^{\star}|^4 |\bar{\boldsymbol{h}}_k^H \bar{\boldsymbol{h}}_k|^2}{\sigma^2 + |\bar{v}_k^{\star}|^2 \bar{\boldsymbol{h}}_k^H \bar{\boldsymbol{h}}_k}\right), \quad (47)
\end{aligned}$$

where the second approximation is due to Assumption 1. Therefore, (34) is proven. The similar derivation can be also applied to the proof of (35), which is omitted here to save space.

Appendix C
Proof of Theorem 2

By introducing $\bar{e}_k = |\bar{v}_k^{\star}|^2 \bar{\boldsymbol{h}}_k^H \bar{\boldsymbol{h}}_k$ and $e_k = |\bar{v}_k^{\star}|^2 \bar{\boldsymbol{h}}_k^H \bar{\boldsymbol{h}}_k$ as the equivalent channel gain between WD k and the FC, we can respectively rewrite (34) and (35) as follows:

$$\begin{aligned}
\bar{\zeta}(\{\bar{v}_k^{\star}\}) &= K - \frac{1}{\sigma^2} \sum_{k\in\mathcal{K}} \left(\bar{e}_k - \frac{\bar{e}_k^2}{\sigma^2 + \bar{e}_k}\right) \\
&= K - \frac{1}{\sigma^2} \sum_{k\in\mathcal{K}} \frac{\sigma^2 \bar{e}_k}{\sigma^2 + \bar{e}_k} \\
&= K - \frac{1}{\sigma^2} \sum_{k\in\mathcal{K}} \frac{\sigma^2}{\sigma^2/\bar{e}_k + 1}, \quad (48)
\end{aligned}$$

$$\zeta(\{\bar{v}_k^{\star}\}) = K - \frac{1}{\sigma^2} \sum_{k\in\mathcal{K}} \frac{\sigma^2}{\sigma^2/e_k + 1}. \quad (49)$$

As we can see, $\bar{\zeta}(\{\bar{v}_k^\star\})$ and $\zeta(\{\bar{v}_k^\star\})$ are monotonically decreasing functions of $\bar{e}_k$ and e_k, respectively. According to the definition of $\bar{e}_k$ and e_k, we have

$$\begin{aligned} e_k &= |\bar{v}_k^\star|^2 \|\mathbf{H}_2\mathbf{\Theta}_2\mathbf{Q}\mathbf{\Theta}_1\boldsymbol{g}_k + \mathbf{H}_2\mathbf{\Theta}_2\tilde{\boldsymbol{g}}_k + \mathbf{H}_1\mathbf{\Theta}_1\boldsymbol{g}_k\|^2 \\ &= |\bar{v}_k^\star|^2 \|\mathbf{H}_2\mathbf{\Theta}_2\mathbf{Q}\mathbf{\Theta}_1\boldsymbol{g}_k + \mathbf{R}_{2,k}\boldsymbol{\theta}_2 + \mathbf{R}_{1,k}\boldsymbol{\theta}_1\|^2 \\ &\overset{(a)}{=} |\bar{v}_k^\star|^2 \|\mathbf{H}_2\mathbf{\Theta}_2\mathbf{Q}\mathbf{\Theta}_1\boldsymbol{g}_k + \bar{\mathbf{R}}_k\bar{\boldsymbol{\theta}}\|^2 \\ &\overset{(b)}{\leq} |\bar{v}_k^\star|^2 (\|\mathbf{H}_2\mathbf{\Theta}_2\mathbf{Q}\mathbf{\Theta}_1\boldsymbol{g}_k\| + \|\bar{\boldsymbol{h}}_k\|)^2, \end{aligned} \tag{50}$$

where (a) is due to Assumption 1 and (b) accrues from the triangle inequality. The equality of (b) holds if and only if the phase vectors of $\mathbf{H}_2\mathbf{\Theta}_2\mathbf{Q}\mathbf{\Theta}_1\boldsymbol{g}_k$ and $\bar{\mathbf{R}}_k\bar{\boldsymbol{\theta}}$ are the same, which can be easily achieved by adjusting the passive beamforming vectors $\boldsymbol{\theta}_1$ and $\boldsymbol{\theta}_2$ at the RISs. Then we have

$$\begin{aligned} e_k &= |\bar{v}_k^\star|^2 (\|\mathbf{H}_2\mathbf{\Theta}_2\mathbf{Q}\mathbf{\Theta}_1\boldsymbol{g}_k\| + \|\bar{\boldsymbol{h}}_k\|)^2 \\ &= |\bar{v}_k^\star|^2 \|\mathbf{H}_2\mathbf{\Theta}_2\mathbf{Q}\mathbf{\Theta}_1\boldsymbol{g}_k\|^2 \\ &\quad + 2|\bar{v}_k^\star|^2 \|\mathbf{H}_2\mathbf{\Theta}_2\mathbf{Q}\mathbf{\Theta}_1\boldsymbol{g}_k\| \|\bar{\boldsymbol{h}}_k\| + \bar{e}_k \\ &\overset{(c)}{\geq} \bar{e}_k, \end{aligned} \tag{51}$$

where the equality of (c) holds if and only if $\|\mathbf{H}_2\mathbf{\Theta}_2\mathbf{Q}\mathbf{\Theta}_1\boldsymbol{g}_k\| = 0$, i.e., the double-reflection links do not exist. Hence, the equivalent channel gain of the DRIS-assisted AirComp system is greater than that of the SRIS-assisted one. In other words, the DRIS-assisted AirComp system can provide less computation MSE. The results follows immediately.

REFERENCES

[1] M. Agiwal, A. Roy, and N. Saxena, "Next generation 5G wireless networks: A comprehensive survey," *IEEE Commun. Surveys Tuts.,* vol. 18, no. 3, pp. 1617-1655, 3rd quater, 2016.

[2] J. Lin, W. Yu, N. Zhang, X. Yang, H. Zhang, and W. Zhao, "A survey on internet of things: Architecture, enabling technologies, security and privacy, and applications," *IEEE Internet Things J.,* vol. 4, no. 5, pp. 1125-1142, Oct. 2017.

[3] X. Chen, D. W. K. Ng, W. Yu, E. G. Larsson, N. Al-Dhahir, and R. Schober, "Massive access for 5G and beyond," *IEEE J. Sel. Areas Commun.,* vol. 39, no. 3, pp. 615-637, Mar. 2021.

[4] X. Cao, G. Zhu, J. Xu, and K. Huang, "Optimal power control for over-the-air computation in fading channels," *IEEE Trans. Wireless Commun.,* vol. 19, no. 11, pp. 7498-7513, Nov. 2020.

[5] W. Liu, X. Zang, Y. Li, and B. Vucetic, "Over-the-Air computation systems: Optimization, analysis and scaling laws," *IEEE Trans. Wireless Commun.*, vol. 19, no. 8, pp. 5488-5502, Aug. 2020.

[6] J.-J. Xiao, S. Cui, Z.-Q. Luo, and A. J. Goldsmith, "Linear coherent decentralized estimation," *IEEE Trans. Signal Process.,* vol. 56, no. 2, pp. 757-770, Feb. 2008.

[7] C.-H. Wang, A. S. Leong, and S. Dey, "Distortion outage minimization and diversity order analysis for coherent multiaccess," *IEEE Trans. Signal Process.,* vol. 59, no. 12, pp. 6144-6159, Dec. 2011.

[8] L. Chen, N. Zhao, Y. Chen, F. R. Yu, and G. Wei, "Over-the-air computation for IoT networks: Computing multiple functions with antenna arrays," *IEEE Internet Things J.,* vol. 5, no. 6, pp. 5296-5306, Dec. 2018.

[9] G. Zhu and K. Huang, "MIMO over-the-air computation for high-mobility multi-modal sensing," *IEEE Internet Things J.,* vol. 6, no. 4, pp. 6089-6103, Aug. 2019.

[10] F. Wu, L. Chen, N. Zhao, Y. Chen, F. R. Yu, and G. Wei, "Computation over wide-band multi-access channels: Achievable rates through sub-function allocation," *IEEE Trans. Wireless Commun.,* vol. 18, no. 7, pp. 3713-3725, Jul. 2019.

[11] L. Chen, N. Zhao, Y. Chen, X. Qin, and F. R. Yu, "Computation over MAC: achievable runction rate maximization in wireless networks," *IEEE Trans. Commun.,* vol. 68, no. 9, pp. 5446-5459, Sep. 2020.

[12] O. Abari, H. Rahul, D. Katabi, and M. Pant, "Airshare: Distributed coherent transmission made seamless," in *Proc. IEEE INFOCOM*, pp. 1742-1750, Apr. 2015.

[13] D. Wen, G. Zhu, and K. Huang, "Reduced-dimension design of MIMO over-the-air computing for data aggregation in clustered IoT networks," *IEEE Trans. Wireless Commun.,* vol. 18, no. 11, pp. 5255-5268, Nov. 2019.

[14] G. Zhu, J. Xu, and K. Huang, "Over-the-air computing for 6G-Turning Air into a computer," [Online]. https://arxiv.org/pdf/2009.02181.pdf, 2020.

[15] M. Gastpar, "Uncoded transmission is exactly optimal for a simple Gaussian 'sensor' network," *IEEE Trans. Inf. Theory,* vol. 54, no. 11, pp. 5247-5251, Nov. 2008.

[16] X. Zhai, X. Chen, J. Xu, and D. W. K. Ng, "Hybrid beamforming for massive MIMO over-the-air computation," *IEEE Trans. Commun.,* vol. 69, no. 4, pp. 2737-2751, Apr. 2021.

[17] Y.-S. Jeon, M. M. Amiri, J. Li, and H. V. Poor, "A compressive sensing approach for federated learning over massive MIMO communication systems," *IEEE Trans. Wireless Commun.,* vol. 20, no. 3, pp. 1990-2004, Mar. 2021.

[18] F. Wu, L. Chen, N. Zhao, Y. Chen, F. R. Yu, and G. Wei, "NOMA-enhanced computation over multi-access channels," *IEEE Trans. Wireless Commun.,* vol. 19, no. 4, pp. 2252-2267, Apr. 2020.

[19] Q. Wu and R. Zhang, "Intelligent reflecting surface enhanced wireless network via joint active and passive beamforming," *IEEE Trans. Wireless Commun.,* vol. 18, no. 11, pp. 5394-5409, Nov. 2019.

[20] Q. Wu and R. Zhang, "Beamforming optimization for wireless network aided by intelligent reflecting surface with discrete phase shifts," *IEEE Trans. Commun.,* vol. 68, no. 3, pp. 1838-1851, Mar. 2020.

[21] C. Huang, A. Zappone, G. C. Alexandropoulos, M. Debbah, and C. Yuen, "Reconfigurable intelligent surfaces for energy efficiency in wireless communication," *IEEE Trans. Wireless Commun.,* vol. 18, no. 8, pp. 4157-4170, Aug. 2019.

[22] M. Di Renzo *et al*., "Smart radio environments empowered by AI reconfigurable meta-surfaces: An idea whose time has come," *EURASIP J. Wireless Commun. Netw.,* May 2019. [Online]. https://doi.org/10.1186/s13638-019-1438-9.

[23] E. Basar, M. Di Renzo, J. De Rosny, M. Debbah, M. Alouini, and R. Zhang, "Wireless communications through reconfigurable intelligent surfaces," *IEEE Access,* vol. 7, pp. 116753-116773, Aug. 2019.

[24] Q. Wu and R. Zhang, "Towards smart and reconfigurable environment: Intelligent reflecting surface aided wireless network," *IEEE Commun. Mag.,* vol. 58, no. 1, pp. 106-112, Nov. 2019.

[25] M. Cui, G. Zhang, and R. Zhang, "Secure wireless communication via intelligent reflecting surface," *IEEE Wireless Commun. Lett.,* vol. 8, no. 5, pp. 1410-1414, Oct. 2019.

[26] D. Xu, X. Yu, Y. Sun, D. W. K. Ng, and R. Schober, "Resource allocation for secure IRS-assisted multiuser MISO systems," in *Proc. IEEE GLOBECOM Wkshps.,* pp. 1-6, Dec. 2019.

[27] X. Guan, Q. Wu, and R. Zhang, "Intelligent reflecting surface assisted secrecy communication: Is artificial noise helpful or not?" *IEEE Wireless Commun. Lett.,* vol. 9, no. 6, pp. 778-782, Jun. 2020.

[28] Q. Wu and R. Zhang, "Weighted sum power maximization for intelligent reflecting surface aided SWIPT," *IEEE Wireless Commun., Lett.,* vol. 9, no. 5, pp. 587-590, May 2020.

[29] C. Pan, H. Ren, K. Wang, M. Elkashlan, A. Nallanathan, J. Wang, and L. Hanzo, "Intelligent reflecting surface enhanced MIMO broadcasting for simultaneous wireless information and power transfer," *IEEE J. Sel. Areas Commun.,* vol. 38, no. 8, pp. 1719-1734, Aug. 2020.

[30] Q. Wu and R. Zhang, "Joint active and passive beamforming optimization for intelligent reflecting surface assisted SWIPT under QoS constraints," *IEEE J. Sel. Areas Commun.,* vol. 38, no. 8, pp. 1735-1748, Aug. 2020.

[31] X. Li, C. Zhang, C. He, G. Chen, and J. A. Chambers, "Sum rate maximization in IRS-assisted wireless power communication networks," *IEEE Internet Things J.,* vol. 8, no. 19, pp. 14959-14970, Oct. 2021.

[32] S. Jung, J.-W. Lee, and C. Lee, "RSS-based channel estimation for IRS-aided wireless energy transfer system," *IEEE Internet Things J.,* vol. 8, no. 19, pp. 14860-14873, Oct. 2021.

[33] Y. Yang, B. Zheng, S. Zhang, and R. Zhang, "Intelligent reflecting surface meets OFDM: Protocol design and rate maximization," *IEEE Trans. Commun.,* vol. 68, no. 7, pp. 4522-4535, Jul. 2020.

[34] B. Zheng and R. Zhang, "Intelligent reflecting surface-enhanced OFDM: Channel estimation and reflection optimization,", *IEEE Wireless Commun. Lett.,* vol. 9, no. 4, pp. 518-522, Apr. 2020.

[35] T. Jiang and Y. Shi, "Over-the-air computation via intelligent reflecting surfaces," in *Proc. IEEE GLOBELCOM,* pp. 1-6, Feb. 2020.

[36] D. Yu, S.-H. Park, O. Simeone, S. S. Shitz, "Optimizing over-the-air computation in IRS-aided C-RAN systems," in *Proc. IEEE SPAWC,* pp. 1-5, Aug. 2020.
[37] Z. Wang, Y. Shi, Y. Zhou, H. Zhou, and N. Zhang, "Wireless-powered over-the-air computation in intelligent reflecting surface aided IoT networks," *IEEE Internet Things J.,* vol. 8, no. 3, pp. 1585-1598, Feb. 2021.
[38] X. Zhai, G. Han, Y. Cai, and L. Hanzo, "Beamforming design based on two-stage stochastic optimization for RIS-assisted over-the-air compuation systems," *IEEE Internet Things J.,* Early Access, Aug. 2021.
[39] B. Zheng, C. You, and R. Zhang, "Double-IRS assisted multi-user MIMO: Cooperative passive beamforming design," *IEEE Trans. Wireless Commun.,* vol. 20, no. 7, pp. 4513-4526, Jul. 2021.
[40] B. Zheng, C. You, and R. Zhang, "Efficient channel estimation for double-IRS aided multi-user MIMO system," *IEEE Trans. Commun.,* vol. 69, no. 6, pp. 3818-3832, Jun. 2021.
[41] C. You, B. Zheng, and R. Zhang, "Wireless communication via double IRS: Channel estimation and passive beamforming designs," *IEEE Wireless Commun. Lett.,* vol. 10, no. 2, pp. 431-435, Feb. 2021.
[42] Q. Shi and M. Hong, "Penalty dual decomposition method for nonsmooth nonconvex optimization-Part I: Algorithms and convergence analysis," *IEEE Trans. Signal Process.,* vol. 68, pp. 4108-4122, Jun. 2020.
[43] M. Goldenbaum and S. Stańczak, "On the channel estimation effort for analog computation over wireless multiple-access channels," *IEEE Wireless Commun. Lett.,* vol. 3, pp. 261-264, Jun. 2014.
[44] M. Soltanalian, M. M. Naghsh, N. Shariati, P. Stoica and B. Hassibi, "Training signal design for correlated massive MIMO channel estimation," *IEEE Trans. Wireless Commun.,* vol. 16, no. 2, pp. 1135-1143, Feb. 2017.
[45] G. Arunabha, J. Zhang, J. G. Andrews, and R. Muhamed, "Fundamentals of LTE," *The Prentice Hall communications engineering and emerging technologies series,* 2010.
[46] M. Goldenbaum, H. Boche, and S. Stańczak, "Nomographic functions: Efficient computaion in clustered Gaussion sensor networks," *IEEE Trans. Wireless Commun.,* vol. 14, no. 4, pp. 2093-2105, Apr. 2015.
[47] M.-M. Zhao, Q. Wu, M.-J. Zhao, and R. Zhang, "Intelligent reflecting surface enhanced wireless networks: Two-timescale beamforming optimization," *IEEE Trans. Wireless Commun.,* vol. 20, no. 1, pp. 2-17, Jan. 2021.
[48] A. Liu, R. Yang, T. Q. S. Quek, and M.-M Zhao, "Two-stage stochastic optimization via primal-dual decomposition and deep unrolling," *IEEE Trans. Signal Process.,* vol. 69, pp. 3000-3015, May 2021.
[49] Q. Shi and M. Hong, "Spectral efficiency optimization for millimeter wave multiuser MIMO systems," *IEEE J. Sel. Topics Signal Process.,* vol. 12, no. 3, pp. 455-468, Jun. 2018.
[50] Q. Wu and R. Zhang, "Intelligent reflecting surface enhanced wireless network: Joint active and passive beamforming design," in *Proc. IEEE GLOBECOM,* Dec. 2018, pp. 1-6.
[51] A. M. C. So, J. Zhang, and Y. Ye, "On approximating complex quadratic optimization problems via semidefinite programming relaxations," *Mathematical Programming,* vol. 110, no. 1, pp. 93-110, Jun. 2007.
[52] T. L. Marzetta, "Noncooperative cellular wireless with unlimited numbers of base station antennas", *IEEE Trans. Wireless Commun.,* vol. 9, no. 11, pp. 3590-3600, Nov. 2010.
[53] K. B. Pertersen and M. S. Pedersen, "The matrix cookbook," Nov. 2012 [Online]. Availabel: https://www.math.uwaterloo.ca/hwolkowi/matrixcookbook.pdf
[54] X. Yu, J.-C. Shen, J. Zhang, and K. B. Letaief, "Alternating minimization algorithms for hybrid precoding in millimeter wave MIMO systems," *IEEE J. Sel. Topics Signal Process.,* vol. 10, no. 3, pp. 485-500, Apr. 2016.

Xiongfei Zhai (M'19) received the B.S. and Ph.D degrees from Zhejiang University, Hangzhou, China, in 2009 and 2018, respectively. He was a visiting student with the Department of Electrical and Computer Engineering, Iowa State University, Ames, IA, USA. He is currently an assistant professor with the School of Information Engineering, Guangdong University of Technology, Guangzhou, China. His research interests include over-the-air computation, massive MIMO communications, millimeter-wave communications, and application of optimization algorithm in communications.

Guojun Han (M'12-SM'14) received his Ph.D. from Sun Yatsen University, Guangzhou, China, and the M.E. degree from South China University of Technology, Guangzhou, China. From March 2011 to August 2013, he was a Research Fellow at the School of Electrical and Electronic Engineering, Nanyang Technological University, Singapore. From October 2013 to April 2014, he was a Research Associate at the Department of Electrical and Electronic Engineering, Hong Kong University of Science and Technology. He is now a Full Professor and Executive Dean at the School of Information Engineering, Guangdong University of Technology, Guangzhou, China. He has been a Senior Member of IEEE since 2014. His research interests are in the areas of wireless communications, signal processing, coding and information theory. He has more than 14 years experience on research and development of advanced channel coding and signal processing algorithms and techniques for various data storage and communication systems.

Yunlong Cai (S'07-M'10-SM'16) received the M.Sc. degree in electronic engineering from the University of Surrey, Guildford, U.K., in 2006, and the Ph.D. degree in electronic engineering from the University of York, York, U.K., in 2010. From 2010 to 2011, he was a Post-Doctoral Fellow with the Electronics and Communications Laboratory, Conservatoire National des Arts et Metiers, Paris, France. Since February 2011, he has been with the College of Information Science and Electronic Engineering, Zhejiang University, Hangzhou, China, where he is currently a Full Professor. From August 2016 to January 2017, he was a Visiting Scholar at the School of Electrical and Computer Engineering, Georgia Institute of Technology, Atlanta, GA, USA. His research interests include transceiver design for multiple-antenna systems, cooperative and relay communications, UAV communications, and machine learning for communications. He is currently an Associate Editor of IEEE SIGNAL PROCESSING LETTERS.

Lajos Hanzo (http://www-mobile.ecs.soton.ac.uk, https://en.wikipedia.org/wiki/Lajos_Hanzo) (FIEEE'04) received his Master degree and Doctorate in 1976 and 1983, respectively from the Technical University (TU) of Budapest. He was also awarded the Doctor of Sciences (DSc) degree by the University of Southampton (2004) and Honorary Doctorates by the TU of Budapest (2009) and by the University of Edinburgh (2015). He is a Foreign Member of the Hungarian Academy of Sciences and a former Editor-in-Chief of the IEEE Press. He has served several terms as Governor of both IEEE ComSoc and of VTS. He has published 1900+ contributions at IEEE Xplore, 19 Wiley-IEEE Press books and has helped the fast-track career of 123 PhD students. Over 40 of them are Professors at various stages of their careers in academia and many of them are leading scientists in the wireless industry. He is also a Fellow of the Royal Academy of Engineering (FREng), of the IET and of EURASIP.